Tke5 is a novel *Pseudomonas putida* toxin that depolarises membranes killing plant pathogens

Carmen Velázquez[1,†], Alejandro Arce-Rodríguez[2,†], Jon Altuna-Alvarez[1], Jessica Rojas-Palomino[3], Andony Flores-Ceron[2], Citlaly Cando-Narvaez[2], Adrián Ruiz[2], Javier De la Peña Noya[2], Amaia González-Magaña[1], María Queralt-Martín[3], Antonio Alcaraz[3], David Albesa-Jové[1,4*] and Patricia Bernal[2*]

[1]Instituto Biofisika (CSIC, UPV/EHU), Fundación Biofísica Bizkaia/Biofisika Bizkaia Fundazioa (FBB), 48940, Leioa, Spain

Departamento de Bioquímica y Biología Molecular, University of the Basque Country, 48940, Leioa, Spain

[2]Departamento de Microbiología, Facultad de Biología, Universidad de Sevilla, 41012, Seville, Spain

[3]Laboratory of Molecular Biophysics, Department of Physics, University Jaume I, 12071, Castellón, Spain

[4]Ikerbasque, Basque Foundation for Science, 48013 Bilbao, Spain

*For correspondence: david.albesa@ehu.eus and pbernal@us.es

[†]These authors have contributed equally to this work.

Running title: Tke5: A new weapon in the *P. putida* arsenal

Keywords: Type VI secretion systems, toxins, immunity proteins, bacterial membranes, plant pathogens, biological control agent, *Pseudomonas putida*

Abbreviations: T6SS, Type VI secretion system; EI pair, effector-immunity pair; UV, ultraviolet; CDD, Conserved Domain Database; 3-*m*Bz, 3-methyl-benzoate; IPTG, β-D-1-thiogalactopyranoside; CFU, colony-forming units.

Author's Note: Two datasets, five supplementary figures and three supplementary tables are attached.

ABSTRACT

The soil bacterium *Pseudomonas putida* injects toxic proteins into neighbouring competitors, including resilient phytopathogens, using the Type VI secretion system (T6SS). The secretion of toxins endows *P. putida* with a significant fitness advantage, allowing this biocontrol agent to thrive in plant-related polymicrobial environments and prevent phytopathogen infections. Despite its agricultural significance, the toxin repertoire of *P. putida*, particularly those secreted via the K2- and K3-T6SSs, remains poorly understood. We present the first comprehensive molecular study of Tke5, a potent toxin encoded within the K3-T6SS, which represents the first comprehensive functional analysis of the BTH_I2691 protein family. Our biophysical data demonstrate that Tke5 is a pore-forming toxin that disrupts bacterial membranes through selective ion transport, inducing membrane depolarisation and cell death. Unlike conventional detergent-like pore-forming toxins, Tke5 preserves overall membrane integrity, avoiding large, non-specific disruptions. This unique mechanism offers a powerful approach to targeting resilient phytopathogens.

This study reveals a previously undescribed mode of action within a widespread yet understudied toxin family. Our findings highlight the potential of *P. putida* as a biocontrol agent, offering alternatives to chemical pesticides by exploiting novel toxin mechanisms. Understanding these bacterial toxins is crucial for developing effective strategies to combat plant pathogens.

INTRODUCTION

Toxins are biochemical substances that can cause disease, death or cellular damage when introduced into or produced within an organism. They interfere with vital cellular processes such as inhibiting enzymatic activities or disrupting metabolism, protein biosynthesis or membrane functions. Among these diverse toxic substances, pore-forming toxins (PFTs) represent a particularly sophisticated class of molecular weapons that have evolved across multiple domains of life, being produced by various organisms, including bacteria, archaea, protozoans, vertebrates, and plants [1,2]. PFTs create pores in target cell membranes, leading to the influx or efflux of ions, small molecules, or proteins through the host membrane, which triggers various secondary responses, including cell death or more subtle manipulation of cell function [3]. PFTs are broadly classified into two categories based on the secondary structures that form the pore: α-PFTs use α-helices to form the transmembrane pore, such as colicins, cytolysin A (ClyA), and actinoporins; and β-PFTs utilise β-sheets/β-barrels to form the pore, which includes *Staphylococcus aureus* α-hemolysin, anthrax toxin or streptolysin O [1,3]. PFTs are soluble proteins that must undergo a transition from the soluble state into a membrane-spanning structure. They bind to the membrane of target cells via specific receptors or non-specific associations with the lipid bilayer. Upon membrane binding, PFT monomers oligomerise, inserting a specific pore-forming motif into the membrane to create a water-filled transmembrane pore. The structural complexity of these pores is evident in their stoichiometry and size, which can vary dramatically: from tetramers to structures involving 50 or more monomers. Consequently, pore dimensions range widely, from as small as 1-2 nm in small β-PFTs to more than 50 nm for large β-PFTs such as the cholesterol-dependent cytolysins (CDCs). The insertion process typically

79 involves significant conformational changes in the protein structure, reflecting the
80 dynamic nature of these molecular pore-forming mechanisms.

81 In bacterial contexts, toxins such as PFTs are often proteins secreted or injected into
82 target cells as part of complex molecular mechanisms of defence or competition and are
83 designed to target eukaryotic host cells or act against rival microorganisms, killing
84 (bactericidal effect) or inhibiting the growth (bacteriostatic) of competing
85 microorganisms. The type VI secretion system (T6SS) represents one of the best-
86 characterised bacterial weapon systems, primarily deploying antimicrobial compounds
87 against Gram-negative bacteria [4]. Its structural components include a cell wall-
88 anchored membrane complex, a baseplate, a contractile sheath-tube assembly, and a
89 spike. Effector proteins are loaded onto specific components, such as the inner Hcp tube
90 and the VgrG-PAAR spike complex, and are ejected upon sheath contraction [5–11]. To
91 ensure loading, T6SS effectors utilise specialised delivery mechanisms. Some effectors
92 are encased in protective Rhs shells, while others rely on chaperones or adaptor
93 proteins, like EagR and Tap. T6SS effector genes typically cluster near structural
94 component genes (*vgrG, PAAR, hcp*) and are often accompanied by their chaperone and
95 adaptor genes. Recent research has identified effector-specific motifs (MIX, FIX, RIX,
96 PIX and WHIX) that are primarily N-terminal domains that facilitate the transport of the
97 C-terminal toxic domain into target cells via the T6SS [12–17].

98 Recent studies have identified several T6SS-dependent PFTs, such as *P. aeruginosa*
99 Tse5, which have a multi-ionic character, exhibiting a preference for cations while
100 remaining permeable to anions [18,19]. Likewise, *P. aeruginosa* Tse4, known for its
101 potent antibacterial activity, promotes cell depolarisation in competing bacteria by
102 incorporating into cellular membranes and forming multi-ionic channels [20].

103 The production of protein toxins by bacteria for competitive advantage comes with a
104 significant challenge: avoiding self-harm. To address this, toxin-producing bacteria have
105 evolved a sophisticated self-protection mechanism. They produce specific immunity
106 proteins that neutralise the effects of their own toxins, creating a crucial safeguard
107 against self-intoxication. These immunity proteins are typically encoded immediately
108 downstream of the toxin gene, forming a toxin-immunity pair. This genetic organisation
109 serves two important functions: it ensures the simultaneous production of both the toxin
110 and the cognate immunity protein, and it allows for the modular integration of the toxin-
111 immunity pairs into diverse secretion systems [21]. While the exact mechanisms of
112 immunity against PFTs are not fully understood, the immunity proteins for these toxins
113 are usually small and hydrophobic, indicating that they likely localise to the cytoplasmic
114 membrane. At this location, they may interfere with pore opening or disrupt the
115 oligomerisation process of the pore-forming toxins [21].

116 The potent antibacterial activity of toxins has led to the exploration of their use in
117 biological control. Many beneficial bacteria, such as some *Pseudomonas* species, act as
118 effective biocontrol agents (BCAs) due to their ability to produce toxins that can inhibit
119 or kill plant pathogens. Biocontrol is of significant importance in modern agriculture,
120 offering a sustainable and environmentally friendly alternative to traditional chemical
121 pesticides. Understanding the underlying mechanisms of toxins, including PFTs, could
122 enhance the development of effective BCAs. In *P. putida*, a plant growth-promoting
123 rhizobacteria (PGPR) well known for its biocontrol ability [22], the T6SS is
124 instrumental in the elimination of severe plant pathogens [23]. *P. putida* KT2440
125 possesses three T6SSs (K1-, K2- and K3-T6SS) and their associated toxins [23], with
126 predicted functions such as nucleases (Tke2, Tke4 and Tke10), pore-forming colicins
127 (Tke6, Tke7, Tke8) or NAD^+/$NADP^+$ hydrolases, *i.e.* Tke1. However, no predicted

128 functions exist for the putative Tke5, Tke9 and Tke3 effectors, and more importantly,
129 none of the ten identified T6SS toxins of this strain have been characterised.
130 Additionally, while the regulation of the K1-T6SS cluster has been thoroughly
131 investigated [23,24], nothing is known about secretion through the K3-T6SS and its
132 predicted associated effector Tke5. The primary reason for this lack of knowledge is that
133 K3-T6SS is not functional under laboratory conditions [23,24], which limits the study of
134 its components.

135 Advancing our understanding of novel toxins and their molecular mechanisms remains
136 crucial for developing effective biocontrol strategies in sustainable agriculture. In this
137 context, our work reveals the mechanism of action of Tke5, a putative T6SS effector of
138 the biocontrol agent *P. putida,* providing the first biophysical characterisation of the
139 BTH_I2691 protein family within the cl49522 superfamily. Tke5 forms ion-selective
140 subnanometric pores in the cytoplasmic membrane of target cells, disrupting ion
141 homeostasis that results in cell depolarisation without compromising membrane
142 integrity. This discovery not only contributes to our fundamental understanding of
143 bacterial competition, but the potent bactericidal activity of Tke5 against
144 phytopathogens also opens new avenues for developing more effective and
145 environmentally friendly crop protection strategies.

146

147 **METHODS**

148 ***Bacterial strains and growth conditions***

149 Bacterial strains are listed in Table S1. Unless otherwise stated, chemicals and reagents,
150 including antibiotics, were purchased from Sigma Aldrich. All strains were grown in
151 Lysogeny broth (LB Lennox; 5 g L^{-1} NaCl) and agar (1.5% w/v) [25] for routine growth

152 with shaking at 180 rpm, as appropriate. *E. coli* strains were incubated at 37°C,
153 phytopathogens at 28ºC and *P. putida* strains at 30°C. Vogel-Bonner Medium (VBM)
154 (200 mg L^{-1} $MgSO_4 \cdot 7H_2O$; 2 g L^{-1} anhydrous citric acid; 10 g L^{-1} K_2HPO_4; 3.5 g L^{-1}
155 $NaNH_4HPO_4 \cdot 4H_2O$; pH 7.0) was used to select transconjugants after triparental
156 conjugation, as *E. coli* donor and helper cells cannot grow using citrate as carbon
157 source. Antibiotics were used at the following concentrations (µg mL^{-1}): rifampicin
158 (Rif), 20 for *P. putida*; kanamycin (Km), 50 for *P. putida*, *Agrobacterium tumefaciens*,
159 *Pectobacterium carotovorum*, *Pseudomonas savastanoi*, *Pseudomonas syringae* and
160 *Dickeya dadantii,* 25 for *E. coli* and *Ralstonia solanacearum,* and 20 for *Xanthomonas*
161 *campestris*; ampicillin (Amp) 100 for *E. coli*, gentamycin (Gm), 25 for *P. putida* and 15
162 for *E. coli*; chloramphenicol (Cm), 10 for *E. coli;* nalidixic acid (Nal), 10 for *E. coli;*
163 streptomycin (Sm), 50 for *E. coli*; tetracycline (Tc), 5 for *E. coli.*

164 ***Construction of plasmids and bacterial strains***

165 Plasmids and primers used in this study are listed in Tables S2 and S3, respectively.
166 DNA manipulations were performed using standard methods [25]. Q5® High-Fidelity
167 DNA polymerase (New England Biolabs) was used for PCR reactions according to the
168 manufacturer's instructions. Primers were synthesised by Macrogen Inc., and restriction
169 enzymes were purchased from New England Biolabs. Plasmid isolation and purification
170 of PCR products were performed with the Plus SV Miniprep DNA Purification System
171 and the Gel and PCR Clean-Up System (Promega), respectively. All DNA constructs
172 were sequenced and verified to be correct before use.

173 Recombinant plasmids were transferred to *E. coli* strains by transformation and to
174 *Pseudomonas, Ralstonia, Agrobacterium, Dickeya, Pectobacterium, Erwinia* and
175 *Xanthomonas* strains by electroporation [26] or conjugation [27], as appropriate.

176 The *tke5* (PP2612) gene was amplified from genomic DNA extracted from *P. putida*
177 KT2440 using primers P1-P2 and P3-P2 (Table S3). Primer P3 is designed to fuse a
178 *pelB* signal sequence at the 5´end. This sequence encodes the 22 amino acids, N-
179 terminal leader peptide MKYLLPTAAAGLLLLAAQPAMA (UniProt Q04085)
180 originally from the Pectate lyase B (PelB) of *Erwinia carotovora* EC [28]. PelB directs
181 the fused protein, Tke5, to the Sec pathway [29]. The *tke5* and *pelB-tke5* genes were
182 cloned into pJET1.2/blunt (Thermo Scientific™), sequenced and then subcloned into
183 the broad host range, medium copy number vector pS238D•M (Table S2, [30]) from the
184 SEVA collection at the NheI/BamHI sites, which excise the *msfGFP* to produce
185 pS238D•*tke5* or pS238D•*pelB-tke5*. Primers P4-P5, that bind up- and downstream
186 pS238D•M insertion site, were used to screen colonies harbouring the insert *pelB-tke5*
187 and for subsequent sequencing.

188 The *tke5* gene was subcloned from pS238D•*tke5* to pCOLADuet™-1 into *mcs-2*,
189 including the TAA stop codon to avoid fusion with the C-terminal S-tag. Subsequently,
190 a tag coding for 9x His residues and a Tobacco Etch Virus (-TEV) cleavage site was
191 cloned upstream *tke5*, resulting in vector pCOLADuet-1•*9xhis-tke5*. These constructs
192 were produced by GenScript service (Table S2).

193 The *tki5* (PP2611) gene, preceded by an artificial RBS region
194 (TTTAAAGGAGATATACAA), was synthesised and cloned into pSEVA424 vector
195 between the KpnI and HindIII restriction sites using GenScript service (Table S2). The
196 RBS and the *tki5* gene were subcloned into the broad host range, low copy number
197 vector pSEVA624C at the KpnI/HindIII sites to produce pSEVA624C•*tki5* (Table S2).
198 Vector pSEVA624C is a derivative of pSEVA621 from the SEVA collection [31,32]
199 constructed in this study, where the $lacI^q$-P_{trc} cargo from pSEVA234C [33] was inserted
200 in the *mcs* of pSEVA621 using PacI/HindIII. Primers P6-P7 were used to screen for the

201 *lacI*^{q}-P_{trc} cargo insertion (Table S3) and primers P8-P9, which bind up- and downstream
202 pSEVA624C *mcs*, to screen colonies harbouring the insert *tki5* and for subsequent
203 sequencing. Vector pSEVA624C has been deposited into NCBI Genbank with accession
204 number PQ628036 and into the SEVA repository https://seva-plasmids.com/ [31,32].

205 ***Bioinformatic analysis***

206 *Pseudomonas tke5* and *tki5* gene sequences and their respective protein product Tke5
207 and Tki5 were obtained from the Pseudomonas Genome database [34].

208 **Sequence homology search - Blast-P**

209 BLASTP analyses were performed at the NCBI website using version 2.16.0 [35] and
210 amino acid sequence searches using SMART [36] and Pfam [37] with the default
211 settings.

212 **Conserved Domain Database - CDD**

213 The CDD from NCBI was used to visualise the conserved domains of proteins Tke5 and
214 Tki5. We accessed this database directly from the output of the BLASTP analyses. The
215 CDD includes NCBI-curated domains, which use 3D-structure information to explicitly
216 define domain boundaries and provide insights into sequence/structure/function
217 relationships, as well as domain models imported from external source databases
218 including Pfam, SMART, COG, PRK and TIGRFAMs [38].

219 **Protein Remote homology detection and 3D structure prediction - HHpred**

220 Additionally, we have used the HHpred server to predict protein homology and 3D
221 structure of Tke5 using the default parameters. This tool is part of the Max Planck
222 Institute (MPI) Bioinformatics Toolkit.

223 **CDART**

224 We used the Conserved Domain Architecture Retrieval Tool (CDART) from the NCBI
225 website to visualise the different architectures present in the BTH_I2691 protein family.

To do so, we introduce the accession number for this domain between brackets [NF041559] in the "Enter Query Protein Sequence" box under "Launch a new search" on the website of this tool. The output was downloaded in a comma-delimited table and is attached to this work as Dataset S1.

Topology –TMHMM-2.0

The topology of Tke5 and Tki5 was predicted using the TMHMM-2.0 algorithm (DTU Health Tech; [39]) with the default settings (Supplementary Fig. 1).

Phylogenetic tree

Protein sequences for phylogenetic analysis were retrieved from the NCBI website after the BLAST-P analysis. The multi-FASTA file was loaded in the Molecular Evolutionary Genetic Analysis (MEGA) tool version 11 [40] for alignment using the ClustalW algorithm. The resulting .mas file was exported as .mega to perform the evolutionary analysis by the Maximum Likelihood method with 500 bootstrap replications and JTT matrix-based model [41] using the same software (MEGA11), exact details as follows, as stated in the software after analysis:

"The evolutionary history was inferred by using the Maximum Likelihood method and JTT matrix-based model [41]. The tree with the highest log likelihood (-133685.63) is shown. Initial tree(s) for the heuristic search were obtained automatically by applying Neighbor-Join and BioNJ algorithms to a matrix of pairwise distances estimated using the JTT model, and then selecting the topology with superior log likelihood value. The tree is drawn to scale, with branch lengths measured in the number of substitutions per site. This analysis involved 71 amino acid sequences. There were a total of 1566 positions in the final dataset. Evolutionary analyses were conducted in MEGA11 [40]".

The resulting file (.mtsx) was exported to a Newick file and loaded into iTOL software [42] for annotation and personalisation at the visualisation level.

251 **Structural-based homology search and protein interactions prediction - AlphaFold**
252 **and Foldseek**

253 The structure of Tke5 was predicted using AlphaFold2 and the PDB file was used as a
254 query to search for homologs based on the structure using Foldseek Search Tool [43]
255 with the default settings.

256 **Multiple Sequence Alignment (MSA) - Clustal Omega and Jalview**

257 VasX from *V. cholerae* serotype O1 (strain ATCC 39315/ El Tor Iaba N16961) with the
258 following identifiers: locus VC_A0020; Uniprot: Q9KNE5 VASX_VIBCH and Tke5
259 (PP2612) from *P. putida* KT2440 were aligned using the Multiple Sequence Alignment
260 (MSA) tool of Clustal Omega (EMBL-EBI) [44] with the default settings and Jalview
261 software was used to visualise the alignment (Supplementary Fig. 2). ChimeraX [45]
262 was used for the visualisation of the AlphaFold predicted 3D structure of Tke5 and
263 VasX.

264 ***Growth inhibition and immunity-driven recovery assays***

265 Cells of *P. putida* KT2440 were electroporated as previously described with a
266 combination of the two compatible plasmids pS238D•M and pSEVA624C or their
267 derivatives harbouring *tke5* or *pelB-tke5* and *tki5*, respectively, as described in Table S2.
268 LB-agar supplemented with Km and Gm was used to select successfully transformed
269 cells. The presence of the plasmid was corroborated by colony PCR using primers P4-
270 P5 and P8-9 (Table S3) for pS238D•M and pSEVA624C derivatives, respectively.

271 To perform the growth curves, overnight cultures of each strain were grown in LB
272 supplemented with the appropriate antibiotics. The next day, the cultures were adjusted
273 to OD_{600} 0.05 in the same medium, and 1 mM of β-D-1-thiogalactopyranoside (IPTG)
274 was added to induce *tki5*. Aliquots of 200 µL were placed in a microtiter plate and the
275 Synergy/H1 microplate reader (Biotek©) was used to measure the OD_{600} every 15 min

276 at 30 ºC. After an initial incubation of 2 h, 0.5 mM of 3-methylbenzoate (3-*m*Bz) was
277 added to each well and cultivated for another 14 h. Data was obtained for three
278 biological replicates, each with technical duplicates.

279 ***Survival growth in the presence of antimicrobial compounds***

280 Overnight cultures of *E. coli* DH5α harbouring the vector pS238D•M [30] or the
281 derivative encoding the PelB-Tke5 effector (pS238D•*pelB-tke5*, Table S2) were grown
282 in LB medium supplemented with Km and diluted in 20 mL of the same medium at
283 OD_{600} of 0.1. A 25 µL sample of each culture was taken at timepoint zero to quantify
284 colony-forming units (CFU) as described below. When required, expression of *pelB-*
285 *tke5* was induced with 0.5 mM 3-*m*Bz. A bactericidal (Gm_{10}) or a bacteriostatic (Tc_5)
286 antibiotic was added to cultures of the control strain *E. coli* pS238D•M for reference to
287 different substances affecting bacterial growth. The cultures were incubated at
288 30 ºC/180 rpm for 6 h, 25 µL samples were taken every hour, and serial dilutions from
289 10^{-1} to 10^{-6} were prepared in a microtiter plate with phosphate buffered saline (PBS). A
290 20 µL aliquot of each dilution was placed onto 120 mm square LB-agar plates in
291 technical duplicates. CFU were determined after 24 and 48h of incubation at 37 ºC. The
292 survival ratio was calculated based on the difference in CFU between each timepoint
293 and timepoint zero, expressed as CFUt=x/CFUt=0. Cellular survival was represented as
294 the Log_{10} of the survival ratio. Three biologically independent experiments were
295 performed.

296 ***Flow cytometry studies of* E. coli *DH5α cells expressing* tke5, pelB-tke5, *and***
297 **tki5**

298 Overnight cultures of *E. coli* DH5α alone or harbouring the vector pS238D (Calles et
299 al., 2019), its derivative encoding the Tke5 (pS238D•*tke5*, Table S2) or PelB-Tke5
300 effector (pS238D•*pelB-tke5*, Table S2) and pSEVA624C•*tki5*, were grown in LB

301 medium supplemented with Km and Gm when appropriate. Genes *tke5* and *pelB-tke5*
302 were induced with 1 mM 3-*m*Bz when the cultures reached OD_{600} of 0.6 and incubated
303 for 2 additional hours in the same conditions. Immunity gene *tki5* was induced with 1
304 mM IPTG for 1 hour before the 3-*m*Bz induction of the effector gene *tke5*. To avoid the
305 leaking expression of the P_{trc}, 0.2% glucose was added to the strains harbouring the
306 pSEVA624C•*tki5* vector. Cultures were diluted in 10 mL of the same medium at OD_{600}
307 of 0.05 and incubated for 2 hours once the 3-*m*Bz was added. Then, bacterial cultures
308 were centrifuged at 6000 g for 15 min at 4 ºC. To perform the flow cytometry studies,
309 the bacterial pellets were resuspended in 1x PBS solution pH 7.4, to reach a final OD_{600}
310 of 0.5.
311 To establish control populations, *E. coli* DH5α cells were subjected to heat shock at
312 85 °C for 5 minutes, followed by cooling at 4 °C for 2 minutes and stained with 4 µM of
313 the fluorescent dye Sytox™ Deep Red to identify the permeabilised population. For the
314 depolarised population, *E. coli* DH5α cells were treated with the antibiotic polymyxin B
315 sulfate (100 µg mL^{-1}) for 30 min and stained with 10 µM of the fluorescent dye
316 $DiBAC_4(3)$. Additionally, *E. coli* DH5α cells harbouring the pS238D vector, with and
317 without 3-*m*Bz induction, were incubated with $DiBAC_4(3)$ and Sytox™ Deep Red to
318 serve as controls for the healthy population (Supplementary Fig. 3a-d). Cells were
319 incubated with the fluorescent dyes for 45 min under constant shaking in dark
320 conditions. Data was collected in the CytoFLEX cytometer with 488 and 638 nm lasers.
321 Channels selected were FITC and APC for $DiBAC_4(3)$ (Exλ = 490 nm, Emλ = 516 nm)
322 and Sytox™ Deep Red (Exλ = 660 nm, Emλ = 682 nm), respectively.
323 *E. coli* DH5α strains harbouring either pS238D•*tke5* or pS238D•*pelB-tke5* or co-
324 transformed with pS238D•*pelB-tke5* and pSEVA624C•*tki5* to assess the neutralisation
325 effect of the immunity gene are shown in Supplementary Fig. 3e-h. Each measurement

326 was performed in triplicate to determine the mean value, and each condition was tested
327 in three-independent experiments (n=3). All data were subsequently analysed using
328 CytExpert.

329 ***Expression and purification of Tke5 to study pore-formation in lipid bilayers***

330 *Escherichia coli* BL21(DE3) cells co-transformed with the pCOLADuet-1•*9xhis-tke5*
331 and pSEVA624C•*tki5* plasmids were grown overnight at 37 °C with agitation in 200
332 mL of LB media supplemented with Km and Gm. For Tke5/Tki5 expression, bacterial
333 cultures were diluted to an initial OD_{600} of 0.1 in 2 L of fresh LB medium supplemented
334 with Km and Gm and induced when the OD_{600} reached 0.7 by adding IPTG to a final
335 concentration of 1 mM. The temperature was lowered to 18 °C, and the bacterial
336 cultures were left overnight in shaking conditions. Cells were harvested by
337 centrifugation at 6000 × g for 20 min, and pellets were stored at −80 °C for subsequent
338 use.

339 The pellet from 4 L of bacterial culture was resuspended in 60 mL of 50 mM Tris–HCl
340 pH 8.0, 500 mM NaCl, 20 mM imidazole (solution A) along with 5 µL of benzonase
341 endonuclease (Millipore, Sigma) and a tablet of protease inhibitor cocktail (cOmplete,
342 EDTA-free, Roche). Cell lysis was performed using sonication with continuous cycles
343 of 15 s ON and 59 s OFF at 60 % amplitude, followed by ultracentrifugation at 125,748
344 × g for 1 hour. The supernatant was filtered through a 0.2 µm membrane and then
345 loaded via a peristaltic pump onto a 5-ml HisTrap HP column (GE Healthcare)
346 equilibrated with solution A.

347 The column was connected to a fast protein liquid chromatography system (ÄKTA
348 FPLC; GE Healthcare) and washed with solution A at 1 mL min^{-1} until the absorbance
349 at 280 nm approached baseline. Tke5 was eluted using 100% solution B (50 mM Tris–
350 HCl pH 8, 500 mM NaCl and 500 mM imidazole) at 3 mL min^{-1}. The central peak

351 fractions were combined, and dithiothreitol (DTT) was added to a final concentration of
352 2 mM. The protein solution was injected into a HiLoad Superdex 200 26/600 pg
353 column, previously equilibrated with 20 mM Tris–HCl pH 8, 150 mM NaCl and 2 mM
354 DTT (solution C). Tke5 eluted as a single monodispersed protein, appearing as a unique
355 band on an SDS–PAGE gel (Supplementary Fig. 4). The identity of the Tke5 band was
356 confirmed by mass spectrometry (Dataset S2). Peak fractions were pooled and
357 concentrated using Amicon centrifugal filter units (30 kDa molecular mass cut-off,
358 Millipore) to a final concentration of 2.5 mg mL^{-1} (*ca*. yield: 1.5 mg L^{-1}) to perform
359 lipid bilayer experiments.

360 ***Study of Tke5 pore-forming activity in planar lipid bilayers***

361 We used the solvent-free modified Montal-Mueller technique to enable the formation of
362 planar lipid membranes in the orifice made over a Teflon film [46]. Lipid preparation
363 involved chloroform evaporation of *E. coli* polar lipid extract (Avanti Polar Lipids;
364 Alabaster, AL) under an argon stream, followed by dissolution in pentane at a
365 concentration of 5 mg mL^{-1}. The *E. coli* polar lipid extract headgroup composition
366 consisted of 67% phosphatidylethanolamine (PE), 23.2% phosphatidylglycerol (PG),
367 and 9.8% cardiolipin (CL), with acyl chains reflecting the intrinsic composition of *E.*
368 *coli* [47].

369 A 20 µL aliquot of lipid solution was added to 1.8 ml of salt solution in both *cis* and
370 *trans* compartments of the Teflon chamber, which was divided by a 15 µm thick Teflon
371 film with a *ca*. 200 µm diameter orifice suitable for bilayer formation (Supplementary
372 Fig. 5). Given the lipophobic nature of the Teflon film, lipid adherence was enhanced
373 by pre-treating the orifice with a 3% hexadecane solution in pentane, which imparts a
374 more lipophilic surface. After pentane evaporation, the salt solution levels in both
375 compartments were raised above the orifice, facilitating planar bilayer formation

through monolayer apposition. Capacitance measurements confirmed appropriate bilayer formation. Two distinct potassium chloride concentration gradients were employed for selectivity measurements: 250 mM KCl *cis* / 50 mM KCl *trans* (250/50 mM) and 50 mM KCl *cis* / 250 mM KCl *trans* (50/250 mM). For conductivity measurements, a symmetrical solution of 150 mM KCl *cis* / 150 mM KCl *trans* (150/150 mM) was used. All solutions were buffered with 5 mM HEPES at pH 7.4, with pH adjustment performed using a GLP22 pH meter (Crison). Tke5, dissolved in 20 mM Tris–HCl (pH 8), 150 mM NaCl, and 2 mM DTT, was added to the *cis* compartment to achieve a final concentration of 50 nM.

Ag/AgCl electrodes were custom-prepared within standard 250 µl pipette tips using 2 M KCl with 1.5% agarose bridges. A potential was considered positive when higher in the *cis* compartment (where the protein was always added), with the *trans* side set to ground. An Axopatch 200B amplifier (Molecular Devices, Sunnyvale, CA) in voltage-clamp mode facilitated current measurement and potential application. Collected data were filtered through an integrated 8-pole Bessel low-pass filter at 10 kHz and recorded with a sampling frequency of 50 kHz using a Digidata 1440A (Molecular Devices, Sunnyvale, CA). Data analysis was performed using pClamp 10 software (Molecular Devices, Sunnyvale, CA). For visualisation, current traces were digitally filtered with 500 Hz using a low-pass 8-pole Bessel filter.

The experimental setup, comprising a membrane chamber and head stage, was isolated from external noise sources by a double metal screen (Amuneal Manufacturing Corp., Philadelphia, PA). This configuration enabled measuring currents in the picoampere range with sub-millisecond time resolution. After potential application, the steady current was determined through Gaussian fitting of current value histograms. Currents

400 were measured across a ± 0-100 mV range at 10 mV intervals, generating a single
401 current-voltage (I-V) curve per experiment.
402 Ion selectivity measurements were conducted using concentration gradients between
403 compartments of either 250/50 mM or 50/250 mM. Tke5-induced currents arise from
404 the presence of at least one selective pore under a salt concentration gradient across
405 compartments. The potential cation or anion preference of Tke5 currents was assessed
406 by measuring the reversal potential (RP), defined as the applied voltage required to
407 nullify the current.
408 A channel's ion selectivity is determined by the RP value: a non-zero RP indicates
409 selective ion transport. For a cation-selective channel, the RP would be negative under
410 the 250/50 mM gradient and positive under the 50/250 mM gradient, with the opposite
411 pattern applying to an anion-selective channel. Obtained RP values, derived from linear
412 regression of measured current-voltage (I-V) curves, were corrected for liquid junction
413 potential using Henderson's equation to eliminate the salt bridge electrode contribution
414 [48]. The corrected RP was subsequently introduced into the Goldman-Hodgkin-Katz
415 (GHK) equation to calculate the channel permeability ratio (P^+/P^-) [49].
416 Channel conductance (G = I/V) was measured using a symmetric potassium chloride
417 concentration of 150 mM/150 mM. Conductance increments (ΔG) were determined at
418 ±100 mV, a voltage at which stable current increments or reductions were consistently
419 observed. These ΔG values were calculated by averaging current increments (ΔI) and
420 dividing by the applied voltage of ±100 mV. Normalised histograms of ΔG, generated
421 with a 2.5 pS bin width, were fit to a single Gaussian distribution to determine the mean
422 ΔG, which corresponded to the minimal channel conductance.

423 ***Plant pathogens growth inhibition assays***

424 Vector pS238D•M or the derivative encoding the PelB-Tke5 effector (pS238D•*pelB-*
425 *tke5*) (Table S2) were transferred to cells of phytopathogens *P. syringae, R.*
426 *solanacearum, A. tumefaciens, D. dadantii, P. carotovorum*, *E. amylovora*, *X.*
427 *campestris* and *P. savastanoi* (Table S1) by conjugation as previously described. VBM
428 agar supplemented with Km was used to select successfully transconjugants. The
429 presence of the plasmids was corroborated by colony PCR using primers P4-P5 (Table
430 S3). Overnight LB Lennox cultures of the abovementioned phytopathogens harbouring
431 pS238D•M or pS238D•*pelB-tke5* were adjusted to an OD_{600} of 0.05 and 200 µL placed
432 into a standard sterile 96 well-plate made of crystal-clear polystyrene with "U" form
433 and 281 µL volume. The viability of the cells (OD_{600nm}) was measured every 15 minutes
434 for 22 hours at 28ºC and 180 rpm using the Synergy/H1 microplate reader by Biotek©.
435 Expression of *pelB-tke5* was induced after 2 hours with 0.5 mM of 3-*m*Bz except for *P.*
436 *savastanoi,* where 0.1 mM was used. 3-*m*Bz was also added to the strains harbouring
437 the *msfGFP* expressing vector pS238D•M to control the intrinsic toxicity of 3-*m*Bz in
438 the absence of the effector. Data was obtained from three biological replicates, each
439 with technical duplicates.

440 ***Statistical analyses***

441 Statistical analyses are based on Student's *t*-tests in which two conditions are compared
442 independently. P-values from raw data were calculated by two-tailed t-test and from
443 ratio data to the control by one-sample t-test using GraphPad Prism 8 version 8.3.0.

444 For flow cytometry assays, the Brown-Forsythe and Welch ANOVA Test with Dunnett's
445 T3 multiple comparison test was performed to assess significant differences between the
446 mean values of independent groups. Statistical significance was indicated as follows:
447 not significant (ns), for $p > 0.05$, * for $p \leq 0.05$, ** for $p \leq 0.01$, *** for $p \leq 0.001$.

448 **RESULTS**

449 ***Tke5 is a putative T6SS-dependent effector***

450 The first study to characterise the T6SSs in *P. putida* identified ten putative T6SS
451 effectors (Tke1 to Tke10) in the KT2440 strain [23]. The study did not determine the
452 function of any of these effectors; although some were predicted to be nucleases (Tke2
453 and Tke4) or colicins (Tke6 and Tke7), the function of others, like Tke5, remained
454 unknown [23]. Our current BLASTP analysis showed that Tke5 is a conserved T6SS
455 component found in the Pseudomonadota phylum (formerly Proteobacteria), belonging
456 to the BTH_I2691 family of the Conserved Domain Database (CDD), with accession
457 number NF041559. A phylogenetic tree using the reference proteins of this NCBI
458 family shows a wide distribution within the Beta- and Gammaproteobacteria classes
459 (Fig. 1a). Most β-proteobacteria were from the Burkholderiales order, while γ-
460 proteobacteria were more diverse, with many representatives from the Pseudomonadales
461 order, but also Vibrionales and Enterobacterales (Fig. 1a). BTH_I2691 protein family is
462 the only member of the recently created superfamily cl49522 (October 2023). In *P.*
463 *putida* Tke5 effector, the BTH_I2691 domain spans amino acids 10 to 858 from a total
464 of 996 amino acids (*E*-value 1.33e-117; Fig. 1b) according to the BLASTP result.
465 Additionally, the CDD revealed a MIX_III domain of the MIX superfamily, also known
466 as the VasX_N superfamily in the Pfam database, which is included within the
467 BTH_I2691 domain. This domain was first identified as a Marker for Type VI effectors
468 [12]. Curiously, it was named VasX_N by the Pfam database because it was present in
469 the N-terminal region of the T6SS effector VasX from *V. cholerae*.

470 VasX is the only member of the family previously identified. It was first described as a
471 virulence factor secreted by *V. cholerae* T6SS necessary to kill the host model system
472 *Dictyostelium discoideum* [50,51]. Subsequently, VasX was shown to be also an

473 antimicrobial effector [51] which compromises the inner membrane of *Vibrio* species,
474 and its activity is neutralised by the cognate immunity protein TsiV2 [50,51]. The
475 effector presented a short domain (775-915 aa from 1085 aa) with homology to a pore-
476 forming colicin also identified in Tke5 (Fig. 1b, dark blue), and preliminary results
477 indicated that VasX compromised membrane integrity [52]. However, the exact
478 mechanism of action of this effector is unknown.

479 The Conserved Domain Architecture Retrieval Tool (CDART) identified 61 different
480 domain architectures within the BTH_I2691 protein family (Dataset S1), where the
481 domain is found alone or in combination with many other domains. BTH_I2691 is
482 mostly identified in the central part of these proteins (ranging from 1000 to 1500 amino
483 acids), and interestingly, on many occasions, their N-terminal domains are also T6SS
484 related. Fig. 1c shows representative proteins identified with CDART containing the
485 T6SS-related domains *i.e.* MIX, PAAR, Tap (DUF4123), DUF2345 (VgrG related),
486 LysM or even VgrG domains. Tke5 is most similar to Architecture number 2, which
487 contains a BTH_I291 covering most of the protein and a single N-terminal MIX domain
488 included in it (Fig. 1b).

489 To infer the function of this T6SS-related domain, we predicted the Tke5 topology that
490 resulted in a 110-kDa membrane protein with five transmembrane domains (See
491 Methods for details, Supplementary Fig. 1a). Moreover, we predicted the putative
492 structure of Tke5 using AlphaFold 2 to perform a structural homology analysis with
493 Foldseek [43]. This analysis retrieved that the Tke5 predicted structure was similar to
494 the structure of *V. cholerae* toxin VasX from the AFDB Swissprot with an E-value of
495 9.82e-22, and the highest probability value (1) (Supplementary Fig. 1b), although the
496 sequence identity was only 21% (Supplementary Fig. 2).

497 The genomic location of *tke5* within the K3-T6SS cluster (Fig. 2a), its structural
498 homology to VasX (Supplementary Fig. 1b), and the presence of an N-terminal MIX
499 domain associated with T6SS-dependent secretion and a C-terminal colicin domain
500 (Fig. 1b) suggest that Tke5 may function as a T6SS-dependent toxin targeting the
501 bacterial membrane.

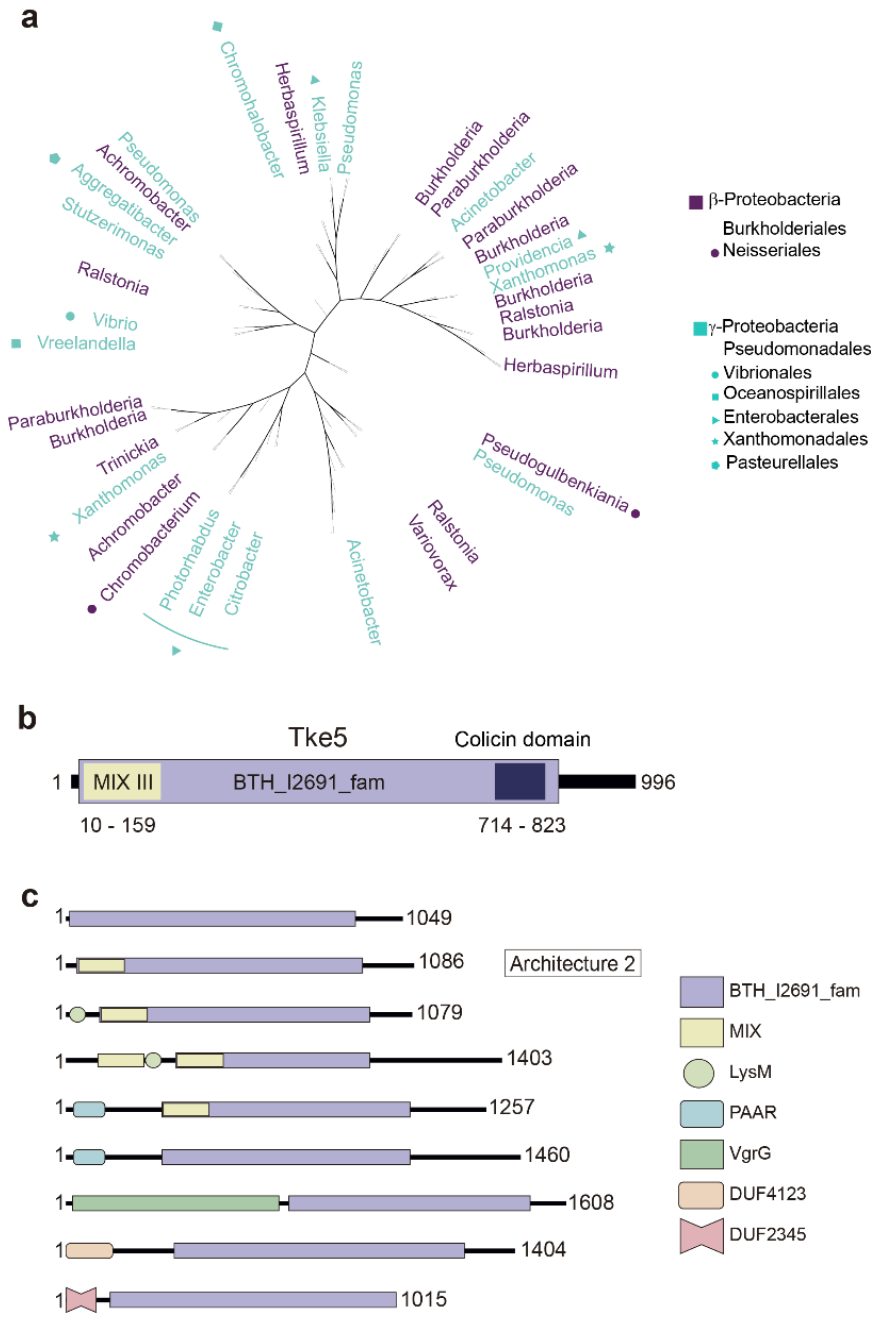

502

503 **Figure 1 |** Tke5 *in silico* study. **a)** Phylogenetic distribution of BTH_I2691 proteins in
504 the Pseudomonadota phylum. A maximum likelihood tree with 500 bootstrap replicates

505 was built with Mega 11 for the reference proteins of the BTH_I2691 family. **b)**
506 Prediction of conserved domains in Tke5 using BLAST-P analysis, showing the spanned
507 amino acids along with the corresponding reference names and identification numbers.
508 **c)** Conserved domain architecture of representative proteins within the BTH_I2691
509 family, indicating the amino acid spans and corresponding reference names.

510

511 ***Tke5 is a potent antimicrobial toxin that can be neutralised by Tki5***

512 To prove that Tke5 is an antimicrobial toxin, we tested the capacity of the putative Tke5
513 effector to impair bacterial growth when heterologously expressed from a plasmid. With
514 this aim, the *tke5* gene was cloned into pS238D•M to produce pS238D•*tke5*.
515 Additionally, a *pelB* sequence was fused to the *tke5* gene and cloned into pS238D•M to
516 produce pS238D•*pelB-tke5*. The signal peptide PelB [53] was used to direct the effector
517 to the Sec pathway to help a possible membrane insertion of Tke5, since the topology
518 analysis revealed transmembrane helices, indicating that this effector might act within
519 the bacterial membranes. The expression vector pS238D•M, known as the digitaliser
520 (ON/OFF), contains a complex regulatory circuit that allows having an OFF state of
521 zero transcription in the absence of induction and thus is ideal for toxin expression [30].
522 The plasmids pS238D•*tke5* and pS238D•*pelB-tke5* were introduced into *P. putida*
523 KT2440, where the K3-T6SS is silent.

524 The expression of the effector gene was induced after two hours of bacterial growth in
525 LB Lennox by the addition of 3-*m*Bz. Upon induction of the putative effector, the
526 growth of the tested strain was significantly impaired, especially when fused to PelB
527 (dark orange and purple curves, Fig. 2b), compared to the same strains harbouring the
528 *msfGFP* reporter gene (light green curve, Fig. 2b). The expression of *msfGFP* was not

529 deleterious, as expected for previous results [30]. These data indicate that Tke5 is a
530 potent antimicrobial toxin (Fig. 2b).

531 Importantly, bacteria with active T6SS require immunity proteins to prevent self-
532 intoxication from their own T6SS antimicrobial effectors and to protect against friendly
533 fire from sister cells. Immunity genes are frequently located downstream of their
534 cognate toxin genes to secure co-expression and thus protection. Therefore, we asked if
535 the gene downstream *tke5, i.e., tki5,* codes for the immunity protein Tki5 (Fig. 2a). To
536 assess the protective functionality of Tki5, the *tki5* gene was cloned into pSEVA624C, a
537 vector compatible with pS238D (Fig. 2b), and then, *P. putida* was transformed with
538 either pS238D•M, pS238D•*tke5* or pS238D•*pelB-tke5*. Expression of the immunity gene
539 (*tki5*) was induced with IPTG at point zero, while the expression of the *tke5* toxin gene
540 was induced with 3-*m*Bz two hours later. The co-expression of the putative *tki5*
541 immunity gene together with the *tke5* or *pelB-tke5* rescued the impaired growth (light
542 orange and purple curves, Fig. 2b). Although Tki5 is predicted to insert into the
543 cytoplasmic membrane (Supplementary Fig. 1c), the expression of the *tki5* immunity
544 gene in *P. putida* KT2440 does not exhibit toxicity (dark green curve, Fig. 2b), which is
545 expected since KT2440 is the natural host of this protein. These data show that Tki5
546 protects *P. putida* KT2440 against Tke5 intoxication, demonstrating that Tke5/Tki5 are
547 an effector-immunity (EI) pair.

548

549 ***Tke5 is a bactericidal antimicrobial toxin***

550 Here, we have demonstrated that Tke5 is a powerful antimicrobial toxin. Depending on
551 their effect on bacterial targets, antimicrobial compounds can be classified as
552 bactericidal if they kill bacteria, or bacteriostatic if they inhibit bacterial growth without
553 directly killing the bacteria (*i.e.*, induce growth arrest). To determine whether Tke5 acts

554 as a bactericidal or bacteriostatic agent, we performed cellular survival assays under the
555 expression of *tke5* using the laboratory host cell *E. coli* DH5α. Two antimicrobial
556 substances with known mechanisms of action were used as controls: the bactericidal
557 antibiotic gentamicin (Gm) and the bacteriostatic antibiotic tetracycline (Tc). Both target
558 the 30S ribosomal subunit binding to the 16S rRNA, but their mechanisms differ
559 significantly. Gm binds irreversibly, fooling the ribosome and leading to indiscriminate
560 tRNAs acceptance, which results in defective proteins and ultimately cell death. In
561 contrast, Tc binds reversibly and prevents the peptide chain elongation. We have
562 represented the cellular survival as the Log_{10} of the survival rate, which is the ratio
563 between the CFU at a given time and the CFU at time zero (Log_{10} survival rate
564 [$CFU_{t=x}/CFU_{t=0}$]). Thus, the cellular survival of an organism growing in the absence of
565 an antimicrobial compound will have a value greater than 0 (*E. coli* harbouring the
566 empty plasmid in the absence of antimicrobial compound, light green curve, Fig. 2c). In
567 the presence of a bacteriostatic agent, the CFU count remains constant over time,
568 resulting in a survival rate of 1 and thus the Log_{10} representing cellular survival is 0 (*E.*
569 *coli* harbouring the empty plasmid in the presence of Tc, dark green empty square curve,
570 Fig. 2c). Conversely, a microorganism exposed to a bactericidal agent will present a
571 cellular survival below 0 (*E. coli* harbouring the empty plasmid in the presence of Gm,
572 dark green full square curve, Fig. 2c). Upon induction of *tke5*, *E. coli* survival at every
573 tested point (hourly for a total of 6 hours) was consistently below 0 as a bactericidal
574 agent (dark purple diamond curve, Fig. 2c), while the uninduced strain (light purple
575 diamond curve, Fig. 2c) reached a cellular survival above 2, showing growth similar to
576 the strain with the empty plasmid.

577 Serial dilutions of these cultures were plated on LB agar plates at points 0, 3 and 6
578 hours to check survival (Fig. 2d). Individual CFU from cultures grown in the absence of

579 antimicrobial compounds were visualised in the dilutions 10-e4 and 10-e5. As expected,
580 the presence of Tc slightly decreased growth but did not kill the population, while no
581 CFU could be visualised in the cultures treated with Gm (Fig. 2d). Confirming the
582 growth curve survival assay, the bactericidal effect of Tke5 was evident at 3 hours upon
583 gene induction, while the non-induced culture grew at the same level as the control
584 strain (Fig. 2d). All this data indicates that Tke5 is a potent bactericidal toxin.

585

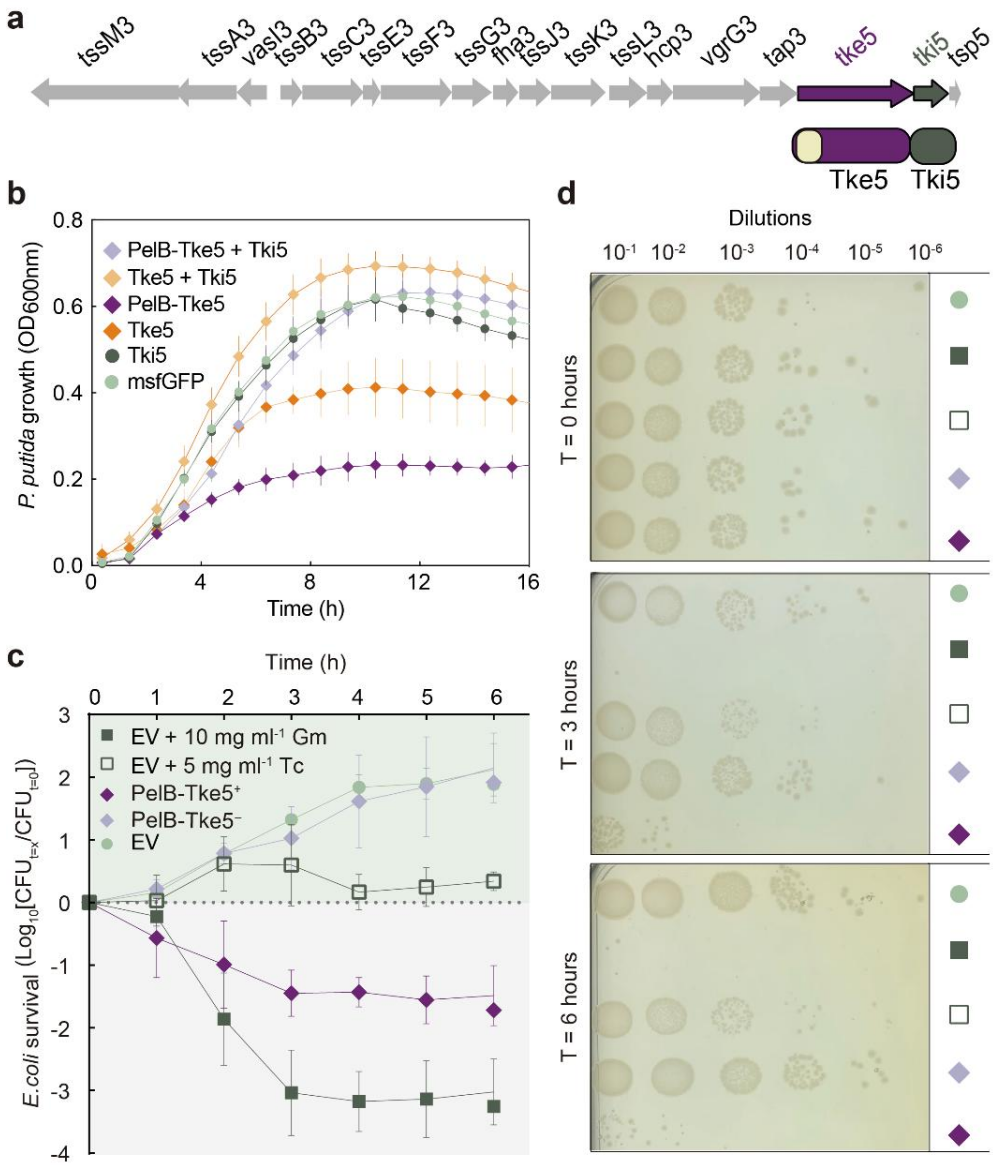

586

587 **Figure 2 |** Tke5 interaction with its cognate immunity pair Tki5 can protect *P. putida* KT2440
588 from self-toxicity. **a)** Schematic representation of the genomic organisation of the genes of the
589 K3-T6SS cluster from *P. putida*. Genes encoding core and accessory components are shown in
590 grey, the *tke5* effector gene is depicted in purple with the MIX domain in yellow and the *tki5*
591 immunity gene is coloured in green. **b)** *P. putida* growth curves under Tke5-Tki5 EI pair
592 production. Overnight cultures were adjusted to OD_{600} 0.1, and the immunity protein was
593 immediately induced with 1 mM IPTG. After 2 h of initial incubation at 30 ºC, effector
594 expression (*tke5* or *pelB-tke5*) was induced by the addition of 0.5 mM 3-*m*Bz (indicated with an
595 arrow). OD_{600} was measured for a total of 16 hours. **c)** Bactericidal activity of Tke5. Survival
596 rate curve of *E. coli* DH5α upon induction of *tke5* expression. CFU survival was quantified over
597 6 h after induction with 0.5 mM 3-*m*Bz. Gentamicin and tetracycline were included for
598 comparison. Bacteria harbouring the *msfGFP*-bearing vector and the recombinant plasmid
599 without induction were used as controls. 20 µL aliquots of each sample were taken hourly to
600 determine the CFU ml^{-1} and calculate the Log_{10} survival rate ($CFU_{t=x}/CFU_{t=0}$). **d)** A subset (0, 3
601 and 6 hours) of each sample of *E. coli* DH5α cells from the different conditions tested in a) were
602 plated in LB-agar to visualise the effect of Tke5 and the different controls on bacterial survival.
603 The experiment was performed in triplicate.

604

605 ***Tke5 induces cell depolarisation that can be neutralised by Tki5***

606 Our data support that Tke5 is a potent bactericidal toxin (Fig. 2b-d) whose toxicity is
607 neutralised by the Tki5 immunity protein (Fig. 2b). Additionally, our bioinformatic
608 analysis suggested that Tke5 could be targeting the bacterial membrane (Supplementary
609 Fig. 1a).

610 To evaluate this possibility, we measured the effect of Tke5 on cell permeability and
611 membrane potential of intoxicated *E. coli* DH5α cells using flow cytometry. To this end,
612 *E. coli* cells were transformed with the plasmid coding for Tke5 (pS238D•*tke5*) or the

613 variant encoding Tke5 fused to the PelB leader sequence (pS238D•*pelB-tke5*). Cells
614 were cultured in liquid media, and the expression of *tke5* or *pelB-tke5* was induced with
615 3-*m*Bz. Two hours after *tke5* induction, cells were stained with Sytox™ Deep Red and
616 $DiBAC_4(3)$ to measure cell permeability and cell depolarisation, respectively. Sytox™
617 Deep Red is a nucleic acid stain that penetrates cells with compromised membranes,
618 resulting in red fluorescence, thus allowing the detection of permeabilised cells by flow
619 cytometry [54]. $DiBAC_4(3)$ is an anionic probe that binds to intracellular proteins or the
620 membrane upon permeation into cells that have lost their resting membrane potential
621 and become depolarised, resulting in green fluorescence [55].

622 To define the possible cell populations resulting from the abovementioned treatment, *i.e.*
623 healthy, permeabilised and depolarised cells, we performed the following controls: i)
624 cell permeabilisation was induced by heat shock (red fluorescence, top left square,
625 Supplementary Fig. 3a), ii) cell depolarisation was induced by treatment with
626 polymyxin B antibiotic (green fluorescence, bottom right square, Supplementary Fig.
627 3b), and iii) untreated cells harbouring the empty pS238D plasmid uninduced and
628 induced with 3-*m*Bz, represented the healthy population (mostly non-fluorescence,
629 bottom left square, although *ca.* 7% showed green fluorescence, bottom right square,
630 Supplementary Fig. 3c and 3d, respectively).

631 Measurements of cells expressing *tke5* and treated with Sytox™ Deep Red and
632 DiBAC4(3) revealed that the production of Tke5 and PelB-Tke5 results in an
633 approximate reduction of 5% and 16% in the healthy cell population, respectively,
634 compared to the negative control (Fig. 3a, Supplementary Fig. 3e and f). These
635 reductions in the healthy population corresponded with an increase in depolarised cells
636 upon Tke5 and PelB-Tke5 induction (Fig. 3b, Supplementary Fig. 3e and f), while the

637 percentage of permeabilised cells (Fig. 3c) or permeabilised and depolarised cells (Fig.
638 3d) remained unchanged and near-zero.

639 These results indicate that Tke5 and PelB-Tke5 alter the membrane potential of
640 intoxicated cells without affecting the integrity of the cytoplasmic membrane.
641 Consistent with our previous data (Fig. 2b), the impact of Tke5 is increased in the
642 presence of the signal peptide PelB (Fig. 3b). As expected, based on results where Tke5
643 toxicity is neutralised by Tki5 (Fig. 2b), co-expression of PelB-Tke5 with the immunity
644 protein Tki5 prevents cell depolarisation (see Methods for details; Fig. 3e-h).

645 Given that our results suggest that Tke5 targets the cytoplasmic membrane of
646 intoxicated cells, causing membrane depolarisation, we hypothesised that Tke5 may be
647 a pore-forming protein that allows ion transport across the membrane, destabilising the
648 resting membrane potential. This ion transport could represent the molecular
649 mechanism employed by Tke5 to depolarise intoxicated cells.

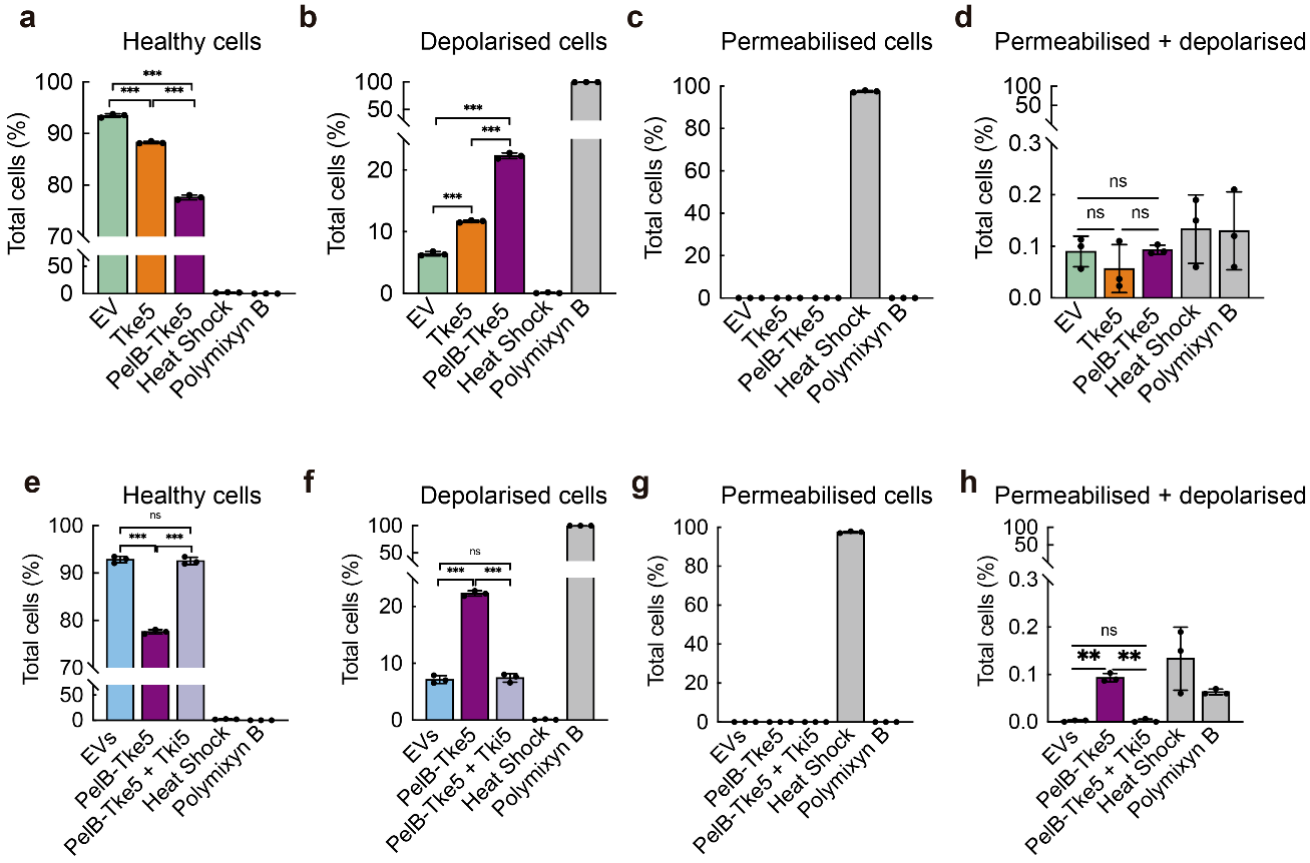

650

651 **Figure 3 |** Cell depolarisation induced by Tke5 effector and toxicity protection from
652 Tki5 immunity protein. Flow cytometry assays were carried out in *E. coli* DH5α cells
653 transformed with the corresponding vectors and stained with both DiBAC4(3)
654 (depolarised population) and Sytox™ Deep Red (permeabilised population). The upper
655 row represents the percentage of healthy (**a**), depolarised (**b**) permeabilised (**c**) and
656 permeabilised + depolarised (**d**) cell populations upon production of Tke5 effector with
657 and without being fused to PelB. Cells with the empty vector, subjected to heat shock
658 and treated with polymyxin B are included as control samples. The bottom row
659 represents the percentage of healthy (**e**), depolarised (**f**), permeabilised (**g**) and
660 permeabilised + depolarised (**h**) cell populations upon expression of PelB-Tke5 effector
661 with and without the co-expression with the immunity protein Tki5. Cells without
662 induction, subjected to heat shock and treated with polymyxin B are included as control
663 samples.

664

665 ***Tke5 forms ion-selective pores in model membranes***

666 To examine the ion channel activity of Tke5, we expressed and purified the protein from
667 the cellular soluble fraction of *E. coli* BL21(DE3) cells co-transformed with
668 pCOLADuet-1•*9xhis-tke5* and pSEVA624C•*tki5* plasmids (see Methods and
669 Supplementary Fig. 4 for details) and evaluated its properties in a model membrane.
670 Importantly, Tke5 is soluble in aqueous solution, exhibiting a dual state, either soluble
671 or membrane-inserted, similar to pore-forming colicins. Using a modified solvent-free
672 Montal-Mueller technique [46], we formed a synthetic lipid bilayer covering a small
673 aperture separating two chambers (*cis* and *trans*) connected to an electric circuit
674 (Supplementary Fig. 5). These chambers, filled with buffers of defined salt
675 concentrations, provide a well-controlled artificial environment using only minimal

676 amounts of material. In contrast to liposomes, one has direct access to both sides of the
677 bilayer and, therefore, it is possible to work in asymmetric conditions in terms of
678 electrolyte and membrane composition. Following protein addition, we can measure
679 ionic currents passing through Tke5-induced membrane pores. This experimental setup
680 allows us to assess the pore conductance and ionic selectivity (cation *versus* anion
681 preference).

682 To start, we assembled the synthetic lipid bilayer using an *E. coli* polar lipid extract in
683 150 mM KCl and confirmed membrane impermeability by ensuring the absence of
684 leakage current. Then we added Tke5 to the *cis* chamber at a final concentration of 50
685 nM and waited for protein insertion until we observed stable currents indicative of ion
686 flow through Tke5-formed pores. Fig. 4a shows a representative current trace (current
687 intensities denoted as I) as a function of applied potential (V). The I/V relationship was
688 linear at low voltages, indicating ohmic behaviour (Fig. 4b, circles), while higher
689 voltages produced small stepwise current jumps (insets in Fig. 4a). Currents in between
690 jumps remained linear (Fig. 4b, squares and diamonds), indicating that the ohmic
691 behaviour was maintained at higher voltages and after the appearance of current jumps.
692 Of note, the frequency of these random transitions between conducting levels increased
693 when the voltage surpassed *ca.* 70 mV, indicating either a change in the number of Tke5
694 pores inserted into the lipid bilayer or, alternatively, dynamic structural changes in the
695 pore size of already existing Tke5 channels.

696 To distinguish between these two possibilities, we first estimated the size of the Tke5
697 pore lumen by applying ±100 mV voltage pulses for long durations and measuring
698 Tke5-induced current jumps (ΔI) (Fig. 4c). We then analysed their respective
699 conductances (ΔG=ΔI/V), which reflect their current-carrying capacity. Histogram in
700 Fig. 4d displays the values obtained and shows a clear peak centred around ΔG = 33 ± 4

701 pS, which aligns with the known conductance in the same salt and lipid conditions of
702 Tse4, another effector secreted by T6SS and recently demonstrated to form narrow ion-
703 selective membrane pores [20]. Tse4 structure is not yet known, but a radius of ~0.5 nm
704 has been estimated for Tse4-induced pores based on electrophysiology data and
705 previous studies showing that small solutes between 300-700 Da (corresponding to 0.45
706 – 0.65 nm equivalent hydrodynamic radius) could not access the cytoplasm of Tse4-
707 intoxicated cells [20,56]. Thus, given the comparable conductance of Tke5 and Tse4 (33
708 pS vs. 20 pS), we can infer a radius of less than 1 nm also for Tke5. Such a
709 subnanometric pore diameter is typical of highly specialised narrow channels allowing
710 only the transport of partially dehydrated ions while excluding larger hydrated ions,
711 other solutes and metabolites [57].

712 The broad conductance range (10-80 pS) observed in Fig. 4d may reflect some
713 variability in the size of Tke5 pores formed among experiments or also the presence of
714 multiple simultaneous insertions operating as clusters. To address this issue, we
715 assessed the ionic selectivity of Tke5-induced pores by measuring the reversal potential
716 (RP) and compared it with the conductance data. The RP is the potential needed to null
717 the current flow through the channel under asymmetric salt conditions [58,59]. Since the
718 physical dimensions of the channel lumen define the intensity of the interaction between
719 the pore charges and the permeating ions, the ionic selectivity of the channel increases
720 as the channel becomes narrower, and vice versa. Accordingly, if the RP necessary to
721 counteract the flow of ions does not change significantly with G, this would mean that a
722 number of quasi-identical channels are inserted simultaneously in the membrane. In
723 contrast, a decrease in RP with increasing G would indicate a size-dependent population
724 of channels [59,60].

725 To study the RP of Tke5 channels, we measured induced currents at two concentration
726 gradients: first with 250 mM KCl in the *cis* chamber and 50 mM KCl in the *trans*
727 chamber (250/50 mM KCl), and then with an inverted gradient of 50/250 mM KCl,
728 (dark blue/light blue data represented in Fig. 4e-h). The gradient mimics the ion
729 concentration differences across bacterial membranes, where total ion concentrations
730 are higher in the periplasm than in the cytosol as a result of charged macromolecules
731 being unable to cross the inner membrane. Representative current traces with the
732 250/50 mM and 50/250 mM KCl gradients are shown in Fig. 4e. For each experimental
733 trace, we plotted the I/V curve (Fig. 4f) to confirm the ohmic behaviour and calculated
734 the conductance associated with each RP measurement (Fig. 4g). In the 250/50 mM KCl
735 gradient, the Tke5 currents produced values of RP ~ 30 mV which is similar to the
736 absolute RP obtained in the 50/250 mM KCl gradient ~ -30. The fact that RP does not
737 change significantly in a variety of Tke5 channels displaying different G values (several
738 orders of magnitude) suggests the presence of clusters of channels with similar
739 dimensions adding to the total ion flow, rather than the assembly of larger pores, which
740 would have altered considerably the RP values in Fig. 4g.

741 The RP also reveals channel selectivity, *i.e.* its relative preference for cations *versus*
742 anions. When a channel favours cations, more positive ions move through the channel
743 from the side with a higher concentration to the side with a lower concentration.
744 Therefore, when the salt concentration is higher on the *cis* side and lower on the *trans*
745 side (250/50 mM KCl gradient), the RP will be negative to counteract the movement of
746 the cations from *cis* to *trans* chambers (note that in our set up the *trans* compartment is
747 grounded, see Methods and Supplementary Fig. 5). Conversely, if the gradient is
748 inverted, the RP will be positive. This is exactly what we observed in our setup, where
749 the average RP for the 250/50 mM KCl gradient is negative (-31±2 mV), while the

750 average RP for the 50/250 mM KCl gradient is positive (+33±3 mV) (Fig. 4g),
751 indicating that Tke5 channels preferentially allow positively charged ions (such as K^+)
752 to flow through.

753 Lastly, to obtain a quantitative estimation of the ratio between the flow of cations and
754 anions, *i.e.* the ion permeability ratio (P_{K^+}/P_{Cl^-}), we used the Goldman-Hodgkin-Katz
755 flux equation (GHK, [61]), which yielded values of P_{K^+}/P_{Cl^-} = 10 ± 3 and 16 ±9 in the
756 250/50 and 50/250 mM KCl gradient, respectively (Fig. 4h), (note that GHK equation
757 shows an exponential relationship between P_{K^+}/P_{Cl^-} and RP, so that small changes in RP
758 yield noticeable differences in P_{K^+}/P_{Cl^-}). Weakly selective channels tend to have a
759 P_{K^+}/P_{Cl^-} <5, while ideal selective channels can reach values of 100-1000 [57,59].
760 Therefore, these results indicate that Tke5 forms subnanometer ionic channels with a
761 relatively high preference for K^+ over Cl^- ions.

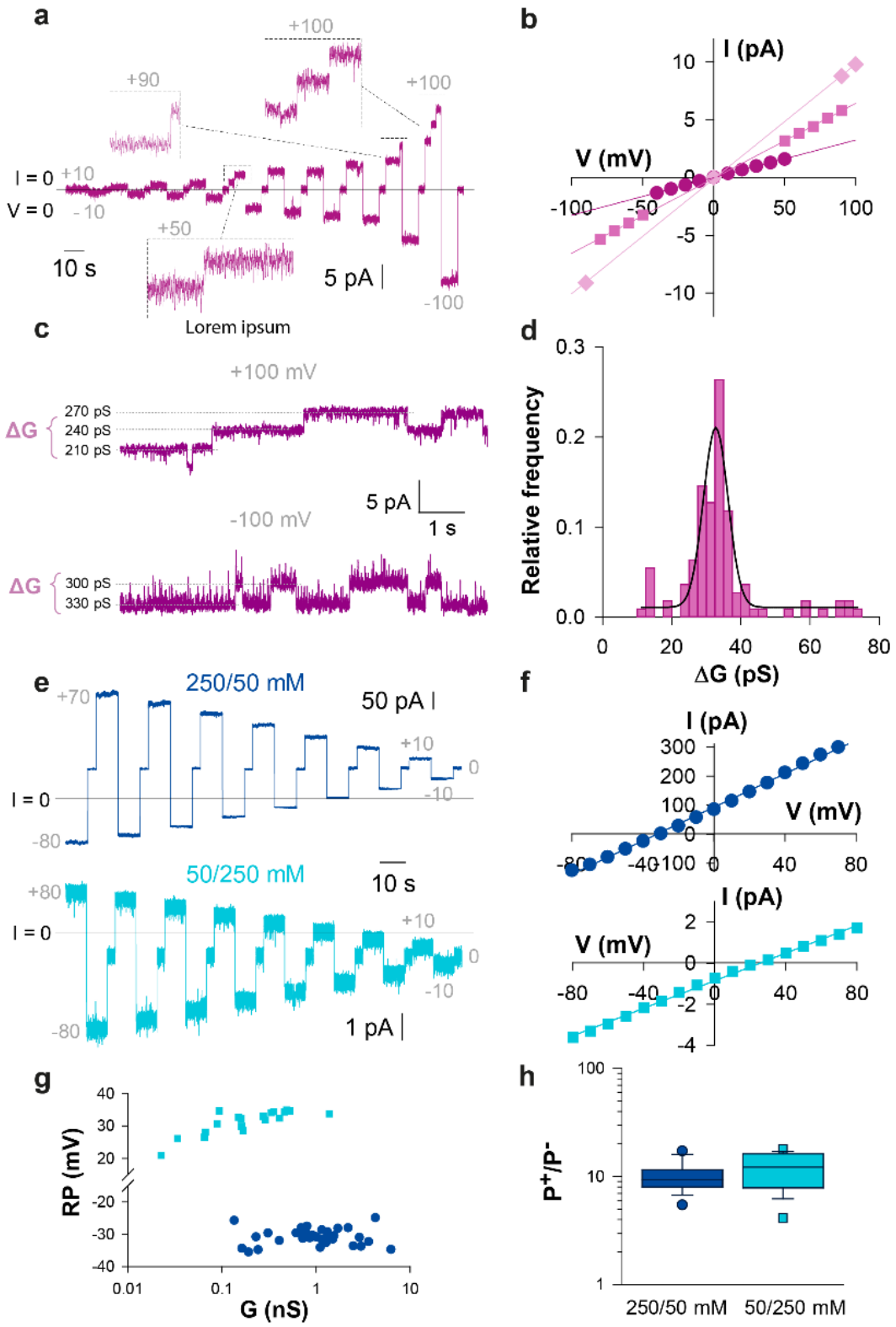

Figure 4 | Tke5 forms stable, cation-selective pores in model membranes. **a)** Representative current trace induced by Tke5 under symmetric 150/150 mM KCl condition. The horizontal black line marks zero applied voltage and zero current.

766 Voltage was applied starting at ±10 mV and increasing it in 10 mV steps up to ±100 mV.
767 Some voltages are indicated in grey. Dashed-lined rectangles highlight current
768 increments at +50, +90 and +100 mV. This trace is representative of 24 independent
769 experiments. **b)** Current-voltage (I/V) plot corresponding to the trace in (a). Solid lines
770 correspond to linear fittings of the experimental data with $R^2 = 0.994$ (circles) and $R^2 =$
771 0.9999 (squares and diamonds). **c)** Representative current traces induced by Tke5 under
772 symmetric 150/150 mM KCl and recorded while maintaining a ±100 mV voltage for
773 long time. Dotted lines indicate the conductance of each level, which are used to
774 calculate the conductance increments $\Delta G = \Delta I / V$, as indicated. This trace is
775 representative of 18 independent experiments. **d**) Normalised histogram (bin of 2.5)
776 showing conductance increments ΔG obtained at ± 100 mV in 150/150 mM KCl as
777 those shown in panel (c). Values are fitted to a Gaussian, with the mean ΔG representing
778 the most probable channel conductance jumps. Histogram built from 110 different
779 current jumps obtained in 18 independent experiments. **e)** Representative stable current
780 traces induced by Tke5 in asymmetric 250/50 mM and 50/250 mM KCl conditions,
781 shown in dark and light blue, respectively. Voltage was applied starting at -80 mV
782 (250/50 mM) or at +80 mV (50/250 mM) and decreased in 10 mV steps down to ±10
783 mV. Some voltages are indicated in grey. The horizontal black line indicates zero
784 current. These traces are representative of 32 (250/50 mM) and 19 (50/250 mM)
785 independent experiments. **f)** I/V plots for traces in (e). **g)** Plot of RP (mV) versus
786 conductance (nS) for independent measurements in 250/50 mM (n=33) and 50/250 mM
787 (n=19) KCl conditions. A negative RP in 250/50 mM KCl gradient condition and a
788 positive RP value in the 50/250 mM KCl gradient condition indicate Tke5 cation
789 selectivity. **h)** Box plot showing cation vs. anion permeability ratios (P^+/P^-) derived

790 from RP values in (**g**). Boxes display the 25th and 75th percentiles, with a line at the
791 median and error bars defining the 10th and 90th percentiles.
792

793 ***The Tke5 toxin kills plant pathogens***

794 *P. putida* is a biocontrol agent that uses the T6SS to kill plant pathogens *i.e.*
795 phytopathogens[23]. Thus, we tested the capacity of the putative Tke5 effector to kill
796 phytopathogens of importance for agriculture. We selected a list of pathogens that
797 included at least one strain of most of the Top 10 plant pathogenic bacteria species
798 based on scientific and economic importance [62] *i.e.,* (1) *Pseudomonas syringae*
799 pathovars; (2) *Ralstonia solanacearum*; (3) *Agrobacterium tumefaciens*; (4)
800 *Xanthomonas oryzae*; (5) *Xanthomonas campestris*; (6) *Xanthomonas axonopodis*; (7)
801 *Erwinia amylovora*; (8) *Xylella fastidiosa*; (9) *Dickeya dadantii*; (10) *Pectobacterium*
802 *carotovorum*, and (11) *Pseudomonas savastanoi*.

803 Among the crops affected by these phytopathogens are brassica crops including
804 broccoli, cauliflower, cabbage, turnip, and mustard (*X. campestris*); coffee, kiwi,
805 tomato, rice, beans, cherry, plum, horse chestnut, loquat (*P. syringae*); carrot, potato,
806 leafy greens, squash, onion, peppers (*P. carotovorum*); walnuts, grapevines, stone fruits,
807 nut trees, sugar beets, horseradish, rhubarb (*A. tumefaciens*) and olive trees, oleander,
808 and ash trees (*P. savastanoi*); the main causal agents are indicated in brackets
809 immediately after the affected crops.

810 To test the efficiency of Tke5 in impairing the growth of plant pathogens, the broad-host
811 range plasmid pS238D•*pelB-tke5* was transferred by conjugation to the strains of
812 interest *i.e.*, *P. syringae* pv. syringae B728a, *R. solanacearum* NCPPB 1493, *A.*
813 *tumefaciens* C58, *D. dadantii* 3937, *P. carotovorum* subsp. carotovorum SCRI 194, *E.*

814 *amylovora* NCPPB 595, *X. campestris* pv vesicatoria NCPPB 195 and *P. savastanoi* pv.
815 savastanoi NCPPB 3335. The expression of the effector gene was induced after two
816 hours of bacterial growth in LB Lennox by the addition of 3-*m*Bz. Upon induction of
817 the putative effector, the growth of the different tested plant pathogens was significantly
818 impaired in all cases (dark purple curve, Fig. 5) compared to their controls, that is, the
819 same strains harbouring the pS238D•M vector (green curves, Fig. 5) or without 3-*m*Bz
820 induction (light purple curve, Fig. 5). The addition of 3-*m*Bz to the plant pathogen
821 strains harbouring the pS238D•M vector, which expresses the *msfGFP* reporter gene
822 instead of the *tke5* gene effector, demonstrated that: i) the concentration of 3-*m*Bz used
823 in our assay is not toxic to these strains, and ii) the level of expression of this system is
824 not inherently toxic, as the production of a non-toxic protein, msfGFP, did not affect the
825 survival of these strains (dark green curve, Fig. 5).

826 All these data demonstrate the potent antibacterial activity of the Tke5 T6SS toxin
827 against a diverse range of economically significant plant pathogens. The broad-
828 spectrum inhibitory effect suggests that Tke5 could be a valuable molecular tool for
829 enhancing the biocontrol capabilities of *P. putida* in agricultural settings. By targeting
830 multiple phytopathogens that threaten crops across various agricultural ecosystems,
831 Tke5 represents a promising strategy for developing more effective and targeted
832 biological control mechanisms.

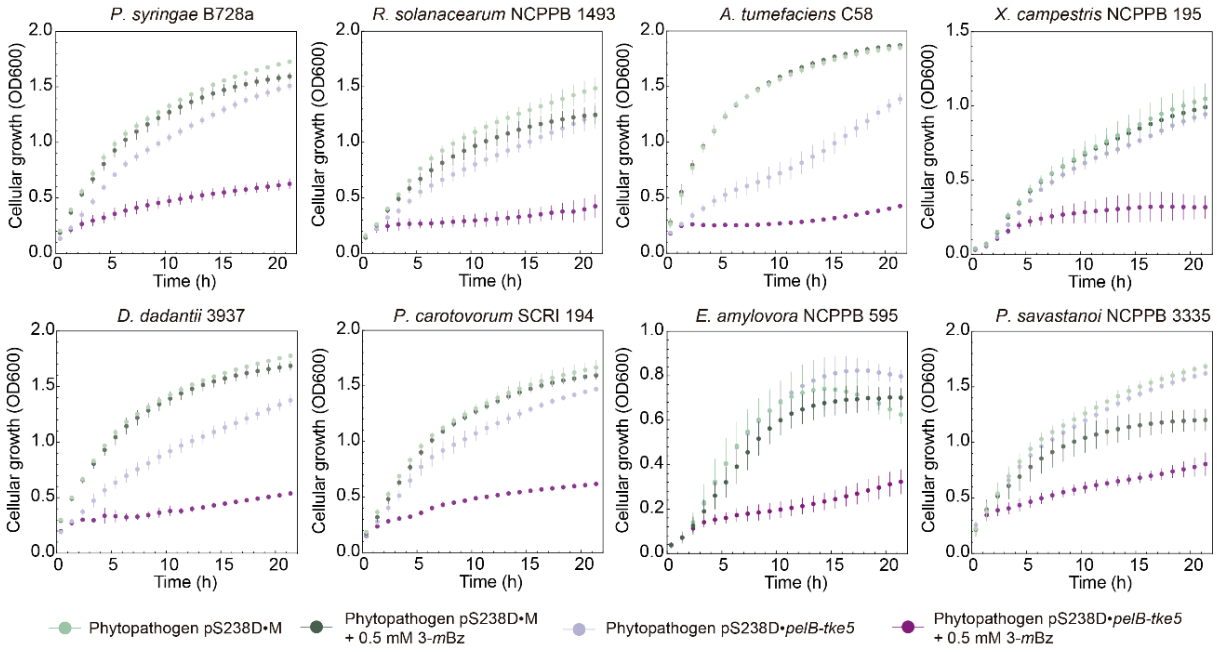

Figure 5 | Toxicity of Tke5 for different recalcitrant phytopathogens. The growth of plant pathogens cells harbouring the pS238D•*pelB-tke5* containing the T6SS effector of *P. putida* Tke5 N-terminal fused to a PelB signal peptide was determined by measuring the OD at 600 nm every 15 minutes for 22 hours at 28ºC using the Synergy/H1 microplate reader by Biotek©. After 2 hours, 3-*m*Bz was added to the LB medium to induce the expression of the *pelB-tke5* gene.

DISCUSSION

The identification and characterisation of novel protein toxins increase our molecular-level understanding of bacterial competition and the dynamics of microbial communities. This can be especially relevant in complex environments like the rhizosphere (surrounding plant roots) and phyllosphere (surrounding plant leaves), where rival bacteria compete to colonise plants [63]. Biocontrol agents in these complex environments, like *P. putida*, use the T6SS as a potent system to eliminate harmful phytopathogen competitors and protect crops from their infections. Here we describe

849 Tke5, a novel potent protein toxin produced by *P. putida* with killing capabilities against
850 the current most recalcitrant phytopathogens.

851 Tke5 is encoded within the K3-T6SS cluster and our bioinformatic analysis suggests it
852 is a conserved T6SS component within the Pseudomonadota phylum (Fig. 1). Tke5
853 represents the first member of the BTH_I2691 family to be comprehensively studied at
854 the molecular level. Another member of this family, VasX, was shown to be a *V.*
855 *cholerae* T6SS-dependent virulence factor crucial to killing *Dictyostelium discoideum*
856 [50] and later studies revealed it also functions as an antimicrobial effector, targeting the
857 inner membrane of other *Vibrio* species leading to depolarisation and subsequent
858 bacterial death [52]. Structural predictions of Tke5 suggest the presence of a MIX_III
859 N-terminal (Fig. 1b), a well-established marker of T6SS effectors [12], which is also
860 predicted in VasX. Additionally, Tke5 is predicted to contain multiple transmembrane
861 domains (Supplementary Fig. 1a), a characteristic also present in VasX, which is
862 associated with its membrane-targeting activity [52].

863 In the present study, we show that Tke5 exhibits potent antibacterial activity in growth
864 inhibition assays using *P. putida* (Fig. 2b). Although we could not perform interbacterial
865 competition assays due to the system's inability to assemble under laboratory
866 conditions, our results show that Tke5 is not merely bacteriostatic but actively kills
867 target bacteria, mirroring the effects of a bactericidal antibiotic (Fig. 2c-d) without
868 provoking cellular lysis. Flow cytometry data indicate that the bactericidal effect is due
869 to cell depolarisation, which occurs without compromising cell permeability, suggesting
870 that Tke5 permeabilises the inner membrane of the bacteria, while maintaining
871 membrane integrity (Fig. 3).

872 To shed some light on the molecular mechanism underlying its cell depolarisation
873 activity, we exploit electrophysiology using an *in vitro* model membrane
874 (Supplementary Fig. 5). The observation of stable currents across the synthetic lipid
875 bilayer upon Tke5 addition provides strong evidence for the formation of ion-selective
876 pores (Fig. 4a-d). Further analysis of the RP under asymmetric salt concentrations
877 (250/50 and 50/250 mM KCl in the cis/trans chambers) reveals that Tke5-induced pores
878 allow the passive multi-ionic transport of ions, but with some preference for cations
879 (K^+) over anions (Cl^-), as indicated by a calculated ion permeability ratio (P_+/P_-) ≈ 10.
880 Furthermore, the RP is constant between traces of varying conductance levels (RP =
881 −31 ±2 mV or +33 ±3 mV in a 250/50 or a 50/250 mM KCl gradient, respectively),
882 which indicates Tke5 assembles a varying number of pores in each experimental
883 replicate, but the structural characteristic of each pore is highly similar (Fig. 4e-g).

884 The capacity of Tke5 to permeate ions across the lipid bilayer is consistent with its cell
885 depolarisation activity. Thus, we would expect that *in vivo*, Tke5 passively transports
886 ions, with some preference for cations, from outside the cell, where they are found at
887 higher concentrations, to inside the cell. This transport disrupts the delicate balance of
888 ions across the membrane, which is crucial for maintaining ionic homeostasis and is
889 essential for preserving the membrane potential and all the cellular processes that
890 depend on it.

891 Several T6SS effectors have been identified that form ion-selective pores in the
892 membranes of target cells, disrupting the membrane potential of the target cell and
893 leading to cell death. Tse4 from *P. aeruginosa* was postulated to act by facilitating the
894 formation of ion-selective membrane pores [64], and we have recently demonstrated
895 that Tse4, indeed, promotes cell depolarisation in prey cells by incorporating into
896 cellular membranes and forming multi-ionic channels [20]. Meanwhile, the C-terminal

897 fragment of Tse5 (Tse5-CT) from the same strain is a PFT that assembles proteolipidic
898 pores in the inner membrane of Gram-negative bacteria [19,65]. In this case, an ion
899 permeability ratio value less than 6 in a 250/50 KCl gradient ($P_+/P_- \leq 6$) was measured
900 using a model membrane with the same lipid composition (the *E. coli* polar lipid
901 extract). Another example is Ssp6, found in *Serratia marcescens*, an antibacterial
902 effector that mainly causes cell depolarisation [66]. For Ssp6, an RP = –26.5 mV was
903 obtained in artificial membranes and non-symmetrical KCl conditions (510/210 mM
904 KCl in *cis* and *trans* chambers, respectively).

905 Recently, a novel family of contact-dependent inhibition (CDI) effectors has been
906 studied in *E. coli* [67]. This new family causes cell depolarisation, while minimal cell
907 permeability was detected. Competition experiments demonstrate that these toxins are
908 highly effective, with ~82% of target cells showing depolarisation in representative
909 assays. However, propidium iodide (PI) uptake, indicating loss of membrane integrity,
910 was observed in only a minor fraction of cells. These results suggest these effectors
911 might also be ionophoric protein toxins that assemble ion-selective membrane pores,
912 causing cell depolarisation.

913 Unlike Tke5 and VasX, which are large proteins with approximately 1,000 amino acids,
914 Tse5-CT, Ssp6, and the C-terminal fragments of CDI toxins represent a contrasting
915 group of small toxins between ~150-230 amino-acid residues. Despite significant
916 differences in size, sequence, and origin, these toxins appear to converge on a similar
917 mode of action, preferentially inserting into the inner membrane of intoxicated bacteria.
918 This shared functional outcome underscores a fascinating case of convergent evolution
919 in toxin mechanisms, likely driven by the same selective pressures to efficiently disrupt
920 bacterial competitors.

921 Tke5 likely employs its N-terminal MIX domain for T6SS-dependent delivery into the
922 target cell, while its C-terminal colicin-like domain is probably involved in causing cell
923 depolarisation through ion channel formation. Our experimental data using synthetic
924 lipid bilayers demonstrate that Tke5 forms stable, ion-selective pores with multi-ionic
925 character and some preference for cations like K^+, presumably destabilising the resting
926 membrane potential of target bacteria. Notably, the measured ion conductance reveals
927 that Tke5 inserts more efficiently under a 250/50 mM salt gradient, where the *cis* side of
928 the bilayer, representing the periplasm, is more shielded than the *trans* side, which
929 mimics the cytoplasm. This setup generates a negative membrane potential simulating
930 physiological conditions, supporting the hypothesis that Tke5 inserts preferentially from
931 the periplasm. Moreover, *in vivo* data show that Tke5 exhibits greater toxicity when
932 directed to the Sec pathway compared to cytoplasmic expression (Fig. 2b), further
933 supporting the periplasmic insertion model. A similar effect has been seen for Tse5,
934 which senses the directionality of the membrane potential and can only release its
935 encapsulated Tse5-CT fragment when introduced in the *cis* chamber under a 250/50 mM
936 salt gradient, and not under a 50/250 mM salt gradient [19]. An even more dramatic
937 effect is seen with Ssp6 from *Serratia*, which is not toxic when overproduced in the
938 cytosol of *E. coli* and only forms ion channels when directed to the Sec translocon or
939 delivered by the T6SS in a competition assay [66].

940 Tki5 expression protects *P. putida* from Tke5 toxicity (Fig. 2 and 3), confirming that
941 Tke5/Tki5 functions as a genuine E/I pair. Tki5 is predicted to be a transmembrane
942 protein (Supplementary Fig. 1c), which suggests it likely interacts with Tke5 at the
943 membrane level to protect *P. putida* from self-intoxication and attack by sibling cells. A
944 similar effect has been shown for VasX and its immunity protein TsiV2 [52]. However,
945 the precise mechanism of this interaction remains to be elucidated.

946 In this study, we also highlight the ecological relevance of Tke5 by demonstrating its
947 potent antibacterial activity against various plant pathogens. Expression of *tke5*
948 significantly impaired growth in multiple phytopathogens, including *P. syringae, R.*
949 *solanacearum, A. tumefaciens, D. dadantii, P. carotovorum, E. amylovora, X.*
950 *campestris,* and *P. savastanoi*, compared to controls (Fig. 5). Control strains carrying
951 empty vector or expressing non-toxic *msfGFP* grew normally with inducer (3-*m*Bz),
952 confirming that growth inhibition stems directly from Tke5 activity. By effectively
953 targeting and neutralising these economically important plant pathogens, Tke5 could
954 play a crucial role in protecting crops and ensuring agricultural productivity. This would
955 add a novel weapon to the *P. putida* arsenal after the already known effectors secreted
956 by the K1-T6SS, such as the Tke2 nuclease [23] and the Tke7 colicin.
957 While T6SS is common in plant-associated bacteria [68], only a few T6SS effectors with
958 biocontrol activity have been characterised. One example is the T6SS amidase $Tae3^{Pf}$
959 from *P. fluorescens* MFE01, which protects against *Pectobacterium atrosepticum* [69].
960 Several beneficial bacteria employ T6SS for plant colonisation and pathogen defence,
961 though their specific effectors remain uncharacterised. For instance, *Azospirillum*
962 *brasilense* T6SS clusters provide antibacterial activity against multiple plant pathogens
963 [70]. Similarly, *Pseudomonas chlororaphis* uses T6SSs to compete against pathogens
964 like *A. tumefaciens* C58 and *P. syringae* pv. tomato DC3000 [71]. The F1- and F3-T6SS
965 in *Pseudomonas ogarae* F113 are crucial for rhizosphere persistence, as demonstrated
966 by the reduced fitness of T6SS-deficient mutants [72]. In *Pseudomonas fluorescens*
967 Pf29Arp, T6SS genes show differential expression between healthy and pathogen-
968 infected wheat roots, suggesting adaptation roles [73]. Even plant pathogens like
969 *Acidovorax citrulli* seem to use T6SS to inhibit other pathogens, reducing rice bacterial
970 blight symptoms caused by *X. oryzae* pv. oryzae [74]. In symbiotic bacteria, T6SS

enhances host colonisation, as seen in the improved competitiveness of *Sinorhizobium freddii* in *G. max* cv Pekin nodules [75].

The characterisation of Tke5 as a novel, pore-forming, bactericidal toxin effector expands our understanding of the sophisticated weaponry employed by bacteria in interbacterial competition. Its activity against plant pathogens further suggests a key role in shaping microbial communities and influencing plant health. This knowledge can inform the development of novel biocontrol strategies and contribute to the ongoing efforts to reduce dependence on chemical pesticides.

ACKNOWLEDGEMENTS

P.B. acknowledges the financial support received from the Spanish Minister of Science, Innovation and Universities (MICIU/AEI/10.13039/501100011033) through the *Ramón y Cajal* Program (RYC2019-026551-I, ESF Investing in your future), the research grant from the State Subprogram for Knowledge Generation PID2021-123000OB-I00 (ERDF/EU) and the research grant from the State Subprogram for Promotion of Research Consolidation CNS2022-135585 (European Union NextGenerationEU/PRTR).

D.A.-J. acknowledges support by the MICIU Contract PID2021-127816NB-I00 and the Basque Government's Department of Education IT1745-22.

A.A. and M.Q.-M. acknowledge financial support by the Spanish Government MICIU/AEI/10.13039/501100011033/FEDER, UE (Project 2019-108434GB-I00 and Project PID2022-142795 NB-I00), Generalitat Valenciana (project CIGRIS/2021/021) and Universitat Jaume I (Project UJI-B2022-42). M.Q.-M acknowledges support from

994 the Spanish Ministry of Science and Innovation (Project IJC2018-035283-I funded by
995 MICIU/AEI/10.13039/501100011033) and Universitat Jaume I (project UJI-A2020-21).

996 We thank Cayo Ramos, Emilia López Solanilla, Francisco M. Cazorla, Ehr Min Lai,
997 María Milagros López and Inmaculada Sampedro for their kind gifts of
998 phytopathogenic strains.

999

1000 **CONFLICTS OF INTEREST STATEMENT**

1001 The authors declare no conflict of interest.

1002

1003 **DATA AVAILABILITY STATEMENT**

1004 The data are available within the manuscript. The sequence of a newly generated vector
1005 available as a tool for the scientific community has been deposited into NCBI Genbank
1006 with accession number PQ628036 and into the SEVA repository https://seva-
1007 plasmids.com/.

1008

1009 **REFERENCES**

1010 1. Mondal AK, Verma P, Lata K, Singh M, Chatterjee S, Chattopadhyay K. Sequence
1011 Diversity in the Pore-Forming Motifs of the Membrane-Damaging Protein Toxins.
1012 Journal of Membrane Biology. Springer; 2020. pp. 469–478. doi:10.1007/s00232-
1013 020-00141-2

1014 2. Carruthers VB. Apicomplexan Pore-Forming Toxins. Annu Rev Microbiol. 2024;78:
1015 277–291. doi:10.1146/annurev-micro-041222

1016 3. Peraro MD, Van Der Goot FG. Pore-forming toxins: Ancient, but never really out of
1017 fashion. Nature Reviews Microbiology. Nature Publishing Group; 2016. pp. 77–92.
1018 doi:10.1038/nrmicro.2015.3

1019 4. Allsopp LP, Bernal P. Killing in the name of: T6SS structure and effector diversity.
1020 Microbiology (N Y). 2023;169: 1367. doi:10.1099/mic.0.001367

1021 5. Rapisarda C, Cherrak Y, Kooger R, Schmidt V, Pellarin R, Logger L, et al. In situ and
1022 high-resolution cryo-EM structure of a bacterial type VI secretion system
1023 membrane complex. EMBO J. 2019;38: e100886. doi:10.15252/embj.2018100886

1024 6. Cherrak Y, Rapisarda C, Pellarin R, Bouvier G, Bardiaux B, Allain F, et al. Biogenesis
1025 and structure of a type VI secretion baseplate. Nat Microbiol. 2018;3: 1404–1416.
1026 doi:10.1038/s41564-018-0260-1 PMID - 30323254

1027 7. Zoued A, Durand E, Brunet YR, Spinelli S, Douzi B, Guzzo M, et al. Priming and
1028 polymerization of a bacterial contractile tail structure. Nature. 2016;531: 59–63.
1029 doi:10.1038/nature17182

1030 8. Kudryashev M, Wang RYR, Brackmann M, Scherer S, Maier T, Baker D, et al.
1031 Structure of the Type VI secretion system contractile sheath. Cell. 2015;160: 952–
1032 962. doi:10.1016/j.cell.2015.01.037

1033 9. Basler M, Pilhofer M, Henderson GP, Jensen GJ, Mekalanos JJ. Type VI secretion
1034 requires a dynamic contractile phage tail-like structure. Nature. 2012;483: 182–
1035 186. doi:10.1038/nature10846

1036 10. Bernal P, Furniss RCD, Fecht S, Leung RCY, Spiga L, Mavridou DAI, et al. A novel
1037 stabilization mechanism for the type VI secretion system sheath. Proc Natl Acad Sci
1038 U S A. 2021;118: e2008500118. doi:10.1073/pnas.2008500118

1039 11. Santin YG, Doan T, Lebrun R, Espinosa L, Journet L, Cascales E. In vivo TssA
1040 proximity labelling during type VI secretion biogenesis reveals TagA as a protein
1041 that stops and holds the sheath. Nat Microbiol. 2018;3: 1304–1313.
1042 doi:10.1038/s41564-018-0234-3

1043 12. Salomon D, Kinch LN, Trudgian DC, Guo X, Klimko JA, Grishin N V., et al. Marker for
1044 type VI secretion system effectors. Proc Natl Acad Sci U S A. 2014;111: 9271–9276.
1045 doi:10.1073/pnas.1406110111

1046 13. Bernal P. T6SS-effector hunters uncover PIX: a novel delivery/marker domain.
1047 Trends Microbiol. 2024;32: 617–619.
1048 doi:https://doi.org/10.1016/j.tim.2024.04.009

1049 14. Kanarek K, Fridman CM, Bosis E, Salomon D. The RIX domain defines a class of
1050 polymorphic T6SS effectors and secreted adaptors. Nat Commun. 2023;14: 4983.
1051 doi:10.1038/s41467-023-40659-2

1052 15. Jana B, Fridman CM, Bosis E, Salomon D. A modular effector with a DNase domain
1053 and a marker for T6SS substrates. Nat Commun. 2019;10: 3595.
1054 doi:10.1038/s41467-019-11546-6

1055 16. Carobbi A, Leo K, Di Nepi S, Bosis E, Salomon D, Sessa G. PIX is an N-terminal
1056 delivery domain that defines a class of polymorphic T6SS effectors in
1057 *Enterobacterales*. Cell Rep. 2024;43: 114015. doi:10.1016/j.celrep.2024.114015

1058 17. Fridman CM, Keppel K, Rudenko V, Altuna-Alvarez J, Albesa-Jové D, Bosis E, et al. A
1059 new class of type VI secretion system effectors can carry two toxic domains and
1060 are recognized through the WHIX motif for export. PLoS Biol. 2025;23.
1061 doi:10.1371/journal.pbio.3003053

1062 18. González-Magaña A, Altuna J, Queralt-Martín M, Largo E, Velázquez C,
1063 Montánchez I, et al. The *P. aeruginosa* effector Tse5 forms membrane pores
1064 disrupting the membrane potential of intoxicated bacteria. Commun Biol. 2022;5:
1065 1189. doi:10.1038/s42003-022-04140-y

1066 19. González-Magaña A, Tascón I, Altuna-Alvarez J, Queralt-Martín M, Colautti J,
1067 Velázquez C, et al. Structural and functional insights into the delivery of a bacterial
1068 Rhs pore-forming toxin to the membrane. Nat Commun. 2023;14: 7808.
1069 doi:10.1038/s41467-023-43585-5

1070 20. Rojas-Palomino J, Velazquez C, Altuna-Alvarez J, Gonzalez-Magana A, Zabala-
1071 Zearreta M, Muller M, et al. The Pseudomonas aeruginosa Tse4 toxin assembles
1072 ion-selective and voltage-sensitive ion channels to couple membrane
1073 depolarization with K+ efflux. PLoS Pathog. 2025;21.
1074 doi:10.1371/journal.ppat.1012981

1075 21. Ruhe ZC, Low DA, Hayes CS. Polymorphic Toxins and Their Immunity Proteins:
1076 Diversity, Evolution, and Mechanisms of Delivery. Annu Rev Microbiol. 2020;74:
1077 497–520. doi:10.1146/annurev-micro-020518

1078 22. Weller DM. *Pseudomonas* Biocontrol Agents of Soilborne Pathogens: Looking Back
1079 Over 30 Years. Phytopathology. 2007;97: 250–256. doi:10.1094/phyto-97-2-0250
1080 PMID - 18944383

1081 23. Bernal P, Allsopp LP, Filloux A, Llamas MA. The *Pseudomonas putida* T6SS is a plant
1082 warden against phytopathogens. ISME Journal. 2017;11: 972–987.
1083 doi:10.1038/ismej.2016.169

1084 24. Bernal P, Civantos C, Pacheco-Sánchez D, Quesada JM, Filloux A, Llamas MA.
1085 Transcriptional organization and regulation of the *Pseudomonas putida* K1 type VI
1086 secretion system gene cluster. Microbiology (N Y). 2023;169: 001295.
1087 doi:10.1099/mic.0.001295

1088 25. Sambrook J, Fritsch EF, Maniatis T. Molecular Cloning: A Laboratory Manual. 2nd
1089 edition. Cold Spring Harbor Laboratory, editor. NY: Molecular Cloning: A Laboratory
1090 Manual; 1989.

1091 26. Choi K-H, Kumar A, Schweizer HP. A 10-min method for preparation of highly
1092 electrocompetent *Pseudomonas aeruginosa* cells: application for DNA fragment
1093 transfer between chromosomes and plasmid transformation. J Microbiol Methods.
1094 2006;64: 391–397. doi:10.1016/j.mimet.2005.06.001

1095 27. Ramos-Gonzalez MI, Duque E, Ramos JL. Conjugational transfer of recombinant
1096 DNA in cultures and in soils: host range of *Pseudomonas putida* TOL plasmids. Appl
1097 Environ Microbiol. 1991;57: 3020–3027.

1098 28. Lei S-P, Lin H-C, Wang S-S, Callaway J, Wilcox G. Characterization of the *Erwinia*
1099 *carotovora pelB* Gene and Its Product Pectate Lyase. J Bacteriol. 1987;169: 4379–
1100 4383. Available: https://journals.asm.org/journal/jb

1101 29. Tsirigotaki A, De Geyter J, Šoštarić N, Economou A, Karamanou S. Protein export
1102 through the bacterial Sec pathway. Nat Rev Microbiol. 2017;15: 21–36.
1103 doi:10.1038/nrmicro.2016.161

1104 30. Calles B, Goñi-Moreno Á, Lorenzo V. Digitalizing heterologous gene expression in
1105 Gram-negative bacteria with a portable ON/OFF module. Mol Syst Biol. 2019;15:
1106 e8777. doi:10.15252/msb.20188777

1107 31. Silva-Rocha R, Martínez-García E, Calles B, Chavarría M, Arce-Rodríguez A, Heras A
1108 de las, et al. The Standard European Vector Architecture (SEVA): a coherent
1109 platform for the analysis and deployment of complex prokaryotic phenotypes.
1110 Nucleic Acids Res. 2013;41: D666–D675. doi:10.1093/nar/gks1119 PMID -
1111 23180763

1112 32. Martínez-García E, Fraile S, Algar E, Aparicio T, Velázquez E, Calles B, et al. SEVA
1113 4.0: an update of the Standard European Vector Architecture database for
1114 advanced analysis and programming of bacterial phenotypes. Nucleic Acids Res.
1115 2023;51: D1558–D1567. doi:10.1093/nar/gkac1059

1116 33. Nikel PI, Benedetti I, Wirth NT, de Lorenzo V, Calles B. Standardization of regulatory
1117 nodes for engineering heterologous gene expression: a feasibility study. Microb
1118 Biotechnol. 2022;15: 2250–2265. doi:10.1111/1751-7915.14063

1119 34. Winsor GL, Griffiths EJ, Lo R, Dhillon BK, Shay JA, Brinkman FSL. Enhanced
1120 annotations and features for comparing thousands of *Pseudomonas* genomes in
1121 the *Pseudomonas* genome database. Nucleic Acids Res. 2016;44: D646–D653.
1122 doi:10.1093/nar/gkv1227

1123 35. Boratyn GM, Camacho C, Cooper PS, Coulouris G, Fong A, Ma N, et al. BLAST: a
1124 more efficient report with usability improvements. Nucleic Acids Res. 2013;41:
1125 W29–W33. doi:10.1093/nar/gkt282

1126 36. Letunic I, Doerks T, Bork P. SMART: Recent updates, new developments and status
1127 in 2015. Nucleic Acids Res. 2015;43: D257–D260. doi:10.1093/nar/gku949

1128 37. Finn RD, Coggill P, Eberhardt RY, Eddy SR, Mistry J, Mitchell AL, et al. The Pfam
1129 protein families database: towards a more sustainable future. Nucleic Acids Res.
1130 2016;44: D279–D285. doi:10.1093/nar/gkv1344 PMID - 26673716

1131 38. Wang J, Chitsaz F, Derbyshire MK, Gonzales NR, Gwadz M, Lu S, et al. The
1132 conserved domain database in 2023. Nucleic Acids Res. 2023;51: D384–D388.
1133 doi:10.1093/NAR/GKAC1096

1134 39. Krogh A, Larsson B, Von Heijne G, Sonnhammer ELL. Predicting transmembrane
1135 protein topology with a hidden markov model: application to complete genomes. J
1136 Mol Biol. 2001;305: 567–580. doi:10.1006/JMBI.2000.4315

1137 40. Tamura K, Stecher G, Kumar S. MEGA11: Molecular Evolutionary Genetics Analysis
1138 Version 11. Mol Biol Evol. 2021;38: 3022–3027. doi:10.1093/MOLBEV/MSAB120

1139 41. Jones DT, Taylor WR, Thornton JM. The rapid generation of mutation data matrices
1140 from protein sequences. Comput Appl Biosci. 1992;8: 275–282.
1141 doi:10.1093/BIOINFORMATICS/8.3.275

1142 42. Letunic I, Bork P. Interactive Tree Of Life (iTOL) v4: recent updates and new
1143 developments. Nucleic Acids Res. 2019;47: W256–W259.
1144 doi:10.1093/NAR/GKZ239

1145 43. van Kempen M, Kim SS, Tumescheit C, Mirdita M, Lee J, Gilchrist CLM, et al. Fast
1146 and accurate protein structure search with Foldseek. Nat Biotechnol. 2024;42:
1147 243–246. doi:10.1038/s41587-023-01773-0

1148 44. Madeira F, Madhusoodanan N, Lee J, Eusebi A, Niewielska A, Tivey ARN, et al. The
1149 EMBL-EBI Job Dispatcher sequence analysis tools framework in 2024. Nucleic Acids
1150 Res. 2024;52: W521–W525. doi:10.1093/nar/gkae241

1151 45. Meng EC, Goddard TD, Pettersen EF, Couch GS, Pearson ZJ, Morris JH, et al. UCSF
1152 ChimeraX: Tools for structure building and analysis. Protein Science. 2023;32:
1153 e4792. doi:10.1002/pro.4792

1154 46. Montal M, Mueller P. Formation of Bimolecular Membranes from Lipid
1155 Monolayers and a Study of Their Electrical Properties. Proceedings of the National
1156 Academy of Sciences. 1972;69: 3561–3566. doi:10.1073/PNAS.69.12.3561

1157 47. Morein S, Andersson A-S, Rilfors L, Ran Lindblom G. Wild-type *Escherichia coli* Cells
1158 Regulate the Membrane Lipid Composition in a "Window" between Gel and Non-
1159 lamellar Structures*. J Biol Chem. 1996;271: 6801–6809.

1160 48. Alcaraz A, Nestorovich EM, López ML, García-Giménez E, Bezrukov SM, Aguilella
1161 VM. Diffusion, exclusion, and specific binding in a large channel: A study of OmpF
1162 selectivity inversion. Biophys J. 2009;96: 56–66. doi:10.1016/j.bpj.2008.09.024

1163 49. Effect THE, Sodium OF, Activity E, The OF. Laboratory, University. 1948; 37–77.

1164 50. Miyata ST, Kitaoka M, Brooks TM, McAuley SB, Pukatzki S. *Vibrio cholerae* Requires
1165 the Type VI Secretion System Virulence Factor VasX To Kill *Dictyostelium*
1166 *discoideum*. Infect Immun. 2011;79: 2941–2949. doi:10.1128/iai.01266-10 PMID -
1167 21555399

1168 51. Dong TG, Ho BT, Yoder-Himes DR, Mekalanos JJ. Identification of T6SS-dependent
1169 effector and immunity proteins by Tn-seq in *Vibrio cholerae*. Proc Natl Acad Sci U S
1170 A. 2013;110: 2623–2628. doi:10.1073/pnas.1222783110

1171 52. Miyata ST, Unterweger D, Rudko SP, Pukatzki S. Dual Expression Profile of Type VI
1172 Secretion System Immunity Genes Protects Pandemic *Vibrio cholerae*. PLoS
1173 Pathog. 2013;9: e1003752. doi:10.1371/journal.ppat.1003752

1174 53. Sockolosky JT, Szoka FC. Periplasmic production via the pET expression system of
1175 soluble, bioactive human growth hormone. Protein Expr Purif. 2013;87: 129–135.
1176 doi:10.1016/J.PEP.2012.11.002

1177 54. Buller GM, Bradford JA, Liu J, Godfrey WL. Novel Reagents for the Addition of
1178 Viability Measurements to Immunostaining Using Flow Cytometry. Blood.
1179 2006;108: 3879–3879. doi:10.1182/BLOOD.V108.11.3879.3879

1180 55. Winkel JD te, Gray DA, Seistrup KH, Hamoen LW, Strahl H. Analysis of antimicrobial-
1181 triggered membrane depolarization using voltage sensitive dyes. Front Cell Dev
1182 Biol. 2016;4: 29. doi:10.3389/FCELL.2016.00029/BIBTEX

1183 56. LaCourse KD, Peterson SB, Kulasekara HD, Radey MC, Kim J, Mougous JD.
1184 Conditional toxicity and synergy drive diversity among antibacterial effectors. Nat
1185 Microbiol. 2018;3: 440–446. doi:10.1038/s41564-018-0113-y

1186 57. Aguilella VM, Queralt-Martín M, Aguilella-Arzo M, Alcaraz A. Insights on the
1187 permeability of wide protein channels: measurement and interpretation of ion
1188 selectivity. Integrative Biology. 2011;3: 159–172. doi:10.1039/C0IB00048E

1189 58. Alcaraz A, Nestorovich EM, López ML, García-Giménez E, Bezrukov SM, Aguilella
1190 VM. Diffusion, exclusion, and specific binding in a large channel: a study of OmpF
1191 selectivity inversion. Biophys J. 2009;96: 56–66. doi:10.1016/J.BPJ.2008.09.024

1192 59. Hille B. Ion Channels of Excitable Membranes. Third Edition. Sunderland, MA, MA:
1193 Sinauer Associates, Inc; 2001.

1194 60. Park HB, Kamcev J, Robeson LM, Elimelech M, Freeman BD. Maximizing the right
1195 stuff: The trade-off between membrane permeability and selectivity. Science
1196 (1979). 2017;356: 1138–1148. doi:10.1126/SCIENCE.AAB0530/ASSET/1FAB46CE-
1197 E045-4C54-80A4-6FD3685D9AEA/ASSETS/GRAPHIC/356_AAB0530_F5.JPEG

1198 61. Hodgkin AL, Katz B. The effect of sodium ions on the electrical activity of the giant
1199 axon of the squid. J Physiol. 1949;108: 37–77.
1200 doi:10.1113/JPHYSIOL.1949.SP004310

1201 62. Mansfield J, Genin S, Magori S, Citovsky V, Sriariyanum M, Ronald P, et al. Top 10
1202 plant pathogenic bacteria in molecular plant pathology. Molecular Plant Pathology.
1203 2012. pp. 614–629. doi:10.1111/j.1364-3703.2012.00804.x

1204 63. Vázquez D, Civantos C, Durán-Wendt D, Ruiz A, Rivilla R, Martín M, et al. The
1205 *Pseudomonas putida* Type VI Secretion Systems Shape the Tomato Rhizosphere
1206 Microbiota. BioRxiv. 2025. doi:10.1101/2025.08.14.670259

1207 64. LaCourse KD, Peterson SB, Kulasekara HD, Radey MC, Kim J, Mougous JD.
1208 Conditional toxicity and synergy drive diversity among antibacterial effectors. Nat
1209 Microbiol. 2018;3: 440–446. doi:10.1038/s41564-018-0113-y

1210 65. Rojas-Palomino J, Altuna-Alvarez J, González-Magaña A, Queralt-Martín M, Albesa-
1211 Jové D, Alcaraz A. Electrophysiological dissection of the ion channel activity of the
1212 Pseudomonas aeruginosa ionophore protein toxin Tse5. Chem Phys Lipids.
1213 2025;267. doi:10.1016/j.chemphyslip.2025.105472

1214 66. Mariano G, Trunk K, Williams DJ, Monlezun L, Strahl H, Pitt SJ, et al. A family of
1215 Type VI secretion system effector proteins that form ion-selective pores. Nat
1216 Commun. 2019;10: 5484. doi:10.1038/s41467-019-13439-0

1217 67. Halvorsen TM, Schroeder KA, Jones AM, Hammarlöf D, Low DA, Koskiniemi S, et al.
1218 Contact-dependent growth inhibition (CDI) systems deploy a large family of
1219 polymorphic ionophoric toxins for inter-bacterial competition. Tan S, editor. PLoS
1220 Genet. 2024;20: e1011494. doi:10.1371/journal.pgen.1011494

1221 68. Bernal P, Llamas MA, Filloux A. Type VI secretion systems in plant-associated
1222 bacteria. Environ Microbiol. 2018;20: 1–15. doi:10.1111/1462-2920.13956

1223 69. Bourigault Y, Dupont CA, Desjardins JB, Doan T, Bouteiller M, Le Guenno H, et al.
1224 *Pseudomonas fluorescens* MFE01 delivers a putative type VI secretion amidase
1225 that confers biocontrol against the soft-rot pathogen *Pectobacterium*

atrosepticum. Environ Microbiol. 2023;25: 2564–2579. doi:10.1111/1462-2920.16492

70. Cassan FD, Coniglio A, Amavizca E, Maroniche G, Cascales E, Bashan Y, et al. The *Azospirillum brasilense* Type VI secretion system promotes cell aggregation, biocontrol protection against phytopathogens and attachment to the microalgae *Chlorella sorokiniana*. Environ Microbiol. 2021;23: 6257–6274. doi:10.1111/1462-2920.15749

71. Boak EN, Kirolos S, Pan H, Pierson LS, Pierson EA. The Type VI Secretion Systems in Plant-Beneficial Bacteria Modulate Prokaryotic and Eukaryotic Interactions in the Rhizosphere. Front Microbiol. 2022;13: 843092. doi:10.3389/fmicb.2022.843092

72. Durán D, Bernal P, Vazquez-Arias D, Blanco-Romero E, Garrido-Sanz D, Redondo-Nieto M, et al. *Pseudomonas fluorescens* F113 type VI secretion systems mediate bacterial killing and adaption to the rhizosphere microbiome. Sci Rep. 2021;11: 5772. doi:10.1038/s41598-021-85218-1

73. Marchi M, Boutin M, Gazengel K, Rispe C, Gauthier J, Guillerm-Erckelboudt A, et al. Genomic analysis of the biocontrol strain *Pseudomonas fluorescens* Pf29Arp with evidence of T3SS and T6SS gene expression on plant roots. Environ Microbiol Rep. 2013;5: 393–403. doi:10.1111/1758-2229.12048 PMID - 23754720

74. Kan Y, Zhang Y, Lin W, Dong T. Differential plant cell responses to *Acidovorax citrulli* T3SS and T6SS reveal an effective strategy for controlling plant-associated pathogens. mBio. 2023;14: e0045923. doi:10.1128/mbio.00459-23

75. Reyes-Pérez PJ, Jiménez-Guerrero I, Sánchez-Reina A, Civantos C, Castro NM, Ollero FJ, et al. The Type VI Secretion System of *Sinorhizobium fredii* USDA257 Is Required for Successful Nodulation With *Glycine max* cv Pekin. Microb Biotechnol. 2025;18: e70112. doi:10.1111/1751-7915.70112